Differential cavitation, angiogenesis and wound-healing responses in injured mouse and rat spinal cords

Surey, Sarina; Berry, Michael; Logan, Ann; Bicknell, Roy; Ahmed, Zubair

DOI:
10.1016/j.neuroscience.2014.06.003

Document Version
Peer reviewed version

Citation for published version (Harvard):
Surey, S, Berry, M, Logan, A, Bicknell, R & Ahmed, Z 2014, 'Differential cavitation, angiogenesis and wound-healing responses in injured mouse and rat spinal cords', Neuroscience, vol. 275, pp. 62-80. https://doi.org/10.1016/j.neuroscience.2014.06.003

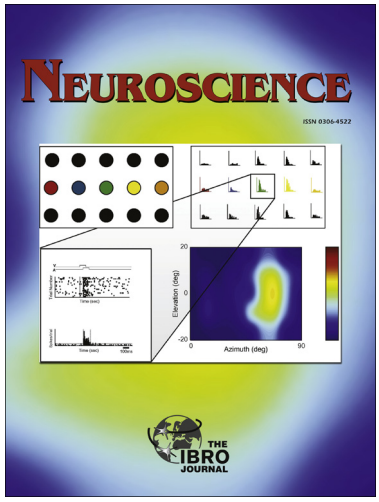

Differential cavitation, angiogenesis and wound healing responses in injured mouse and rat spinal cords

S. Surey, M. Berry, A. Logan, R. Bicknell, Z. Ahmed

PII: S0306-4522(14)00486-2
DOI: http://dx.doi.org/10.1016/j.neuroscience.2014.06.003
Reference: NSC 15472

To appear in: *Neuroscience*

Accepted Date: 4 June 2014

Please cite this article as: S. Surey, M. Berry, A. Logan, R. Bicknell, Z. Ahmed, Differential cavitation, angiogenesis and wound healing responses in injured mouse and rat spinal cords, *Neuroscience* (2014), doi: http://dx.doi.org/10.1016/j.neuroscience.2014.06.003

Differential cavitation, angiogenesis and wound healing responses in injured mouse and rat spinal cords

S. SUREY[1], M. BERRY[1], A. LOGAN[1], R. BICKNELL[2] and Z. AHMED[*]

[1]Neurotrauma and Neurodegeneration Section, School of Clinical and Experimental Medicine, University of Birmingham, Birmingham, B15 2TT

[2]CRUK Molecular Angiogenesis Group, School of Immunity and Infection, University of Birmingham, Birmingham, B15 2TT

***Correspondence to:** Dr. Zubair Ahmed, Neurodegeneration and Neurotrauma, School of Clinical and Experimental Medicine, College of Medical and Dental Sciences, University of Birmingham, Room WX2.17 Institute of Biomedical Research (West), Edgbaston, Birmingham B15 2TT, UK. Tel: +(44) 121 4148858, Fax: +(44) 121 414 8867, Email: z.ahmed.1@bham.ac.uk.

ABSTRACT

The vascular disruption, blood vessel loss and cavitation that occur at spinal cord injury (SCI) epicentres in mice and rats are different, but few studies have compared the acute SCI response in the two species. This is of interest since key elements of the rat SCI response are shared with humans. In this study, we investigated acute SCI responses and characterised changes in pro- and anti-angiogenic factors and matrix deposition in both species. Cavitation was absent in mouse but the area of the lesion site was 21- and 27-fold larger at 8 and 15 days post lesion (dpl), respectively, in the rat compared to intact control. The absence of wound cavitation in the mouse was correlated with increased levels of immunoreactive pro-angiogenic, pro-matrix and pro-wound healing factors, e.g. laminin, matrix metalloproteinase-1 (MMP-1) and vascular endothelial growth factor-A (VEGF-A) within the wound, which were 6.0-, 2.9-, and 2.8-fold, respectively, higher in the mouse compared to rats at 8 dpl. Increased axonal sparing was observed after DC injury, detected by higher levels of PKC-γ immunoreactivity in the dorsal column of mice compared to rats at both T7 and T9 spinal segments. Despite similar post SCI deficits in plantar heat tests at 2 hours after injury (1.4- and 1.6-fold lower than control mice and rats, respectively), by 7 days the magnitude of these responses were comparable to sham-treated controls in both species, while no post-SCI changes in Von Frey hair filament test response were observed in either species. We conclude that the more robust angiogenesis/wound healing response in the mouse attenuates post-injury wound cavitation. Although the spinal cord functions that were monitored post-injury were similarly affected in both species, we suggest that the quality of the angiogenesis/wound healing response together with the diminished lesion size seen after mouse SCI may protect against secondary axon damage and create an

environment more conducive to axon sprouting/regeneration. These results suggest the potential therapeutic utility of manipulating the angiogenic response after human SCI.

Key words: spinal cord injury, wound healing, cavitation, angiogenesis, mouse, rat.

INTRODUCTION

Secondary damage after spinal cord injury (SCI) induces a cascade of injury responses including astrocyte reactivity and haematogenous immune cell immigration that contribute to ischemia, necrosis, oedema, apoptosis and cavitation, which compromise vascular and blood-brain barrier (BBB) integrity and disrupt motor, sensory and reflex pathways (Bazley et al., 2012; Fujiyoshi et al., 2007). New blood vessels formed in the wound by angiogenesis from pre-existing vessels, deliver the oxygen and nutrients that are essential to SCI wound repair (Oudega, 2012). Attempts at therapeutic correction of the vascular disruption after SCI (Casella et al., 2006; Casella et al., 2002; Dray et al., 2009; Whetstone et al., 2003), have utilised pro-angiogenic factors including VEGF-A (Benton et al., 2009; Benton and Whittemore, 2003; Sundberg et al., 2011; Widenfalk et al., 2003), angiopoietins (Han et al., 2010; Herrera et al., 2010), FGF1 and 2 (De Laporte et al., 2011; Goldshmit et al., 2012; Nordblom et al., 2012) and TGF-β1 and 2 (De Laporte et al., 2011; Han et al., 2010; Kohta et al., 2009).

Although it is generally accepted that mice and rats exhibit different responses to SCI (Byrnes et al., 2010; Inman and Steward, 2003; Sroga et al., 2003), both species are commonly used as research tools in comparable studies of CNS repair after SCI. Differences between the two species include the inflammatory response; e.g. the increased numbers of T-cells peak at 3-7 days after injury in rats while, in mice, T-cell numbers peak later at 14 days (Byrnes et al., 2010; Sroga et al., 2003). Larger wound cavities develop in rats compared to mice, suggesting that wound healing and scarring responses are also different (Byrnes et al., 2010). Type I and II SCI wound cavities are recognised. The former are in continuity with the subarachnoid space and contain ECM proteins laminin and collagen, whereas the

latter contain mainly inflammatory cells, no ECM proteins and are discontinuous with the subarachnoid space (Fitch et al., 1999; Lagord et al., 2002).

We hypothesised that, since wound cavitation after SCI is less developed in mice than in rats, mice have an accelerated acute wound healing response characterised by rapid re-vascularisation and matrix deposition. We used laminin immunoreactivity as a surrogate marker for this enhanced healing response and identified the time-point at which significant differences arose between these species. We then used the identified time-point to conduct a detailed investigation into the differences in pro-/anti-angiogenic and ECM molecule production in the two species after DC injury. Accordingly, we predicted that compared to rats, mice would have higher levels of pro-angiogenic VEGF-A, laminin and fibronectin expression in the acute phase of scarring and that the preservation of structure engendered by rapid healing and reduced cavitation in mice would correlate with enhanced levels of immunoreactivity for PKC-γ, indicative of enhanced neuropil sparing compared to rats. Furthermore, we predicted that the responses to thermal and mechanical stimuli would be more significantly affected by SCI in rats than in mice.

EXPERIMENTAL PROCEDURES

Ethics statement

This study was carried out in strict accordance to the UK Animals Scientific Procedures Act, 1986 and all procedures were licensed and approved by the UK Home Office. The protocols and experiments were also approved by the University of Birmingham Ethical Review Sub-Committee. All surgery was performed under inhalation anaesthesia using 5% Isofluorane (IsoFlo, Abbott Animal Health, North Chicago, IL, USA) for induction and 2% for maintenance. Animals were kept in environmentally controlled animal facilities at the University of Birmingham and every effort was made to minimise animal suffering.

Experimental design

Type of analysis	N - numbers	End-points (days)
Cavitation over time	6 (per time point/species)	0, 2, 8, 15
Laminin timeline	6 (per time point/species)	0, 2, 8, 15
Angiogenic/wound healing Immunohistochemistry	6 (per time point/species)	0, 8
Angiogenic/wound healing Western blot analysis	6 (per time point/species)	0, 8
Functional tests	6 (per species/group)	-1 (day before), 0 (2hrs after surgery), 7, 14, 21

Surgical procedures

Three groups containing 6 adult female Sprague-Dawley rats (180-250g) or 6 adult female C57BL6 mice (20-25g) (Charles River, Margate, UK), comprised; Group 1 - sham operated (laminectomy only); Group 2 - dorsal column (DC) crush; and Group 3 - intact controls. DC crush was performed as described by us previously (Ahmed et al., 2010; Lagord et al., 2002). Briefly, animals were anaesthetised using 5% isoflurane with 1.8l/min of oxygen, and given a subcutaneous injection of the

analgesic Buprenorphine before surgery. After laminectomy, DC were crushed bilaterally at the level of T8. The tips of calibrated watchmaker's forceps separated by 1 mm were inserted through the dorsal cord meninges to a depth of 1 mm in rats and separated by 0.5mm in mice to a depth of 0.45 mm. These differences in injury sizes between rats and mice were calculated according to the Christopher & Dana Reeve Foundation spinal cord atlas for T8 level and represented equivalent DC injury sites in both species.

Animals were randomly assigned, the identity of each animal was blinded by a second investigator, and randomly allocated to times of sacrifice post-SCI and portions of the cord at T8, encompassing the SCI site were harvested for analysis. For histology and immunohistochemistry, animals were killed in increasing concentrations of CO_2 and intracardially perfused with 4% paraformaldehyde (PFA; TAAB Laboratories, Berkshire, UK). A 1 cm length of the spinal cord (0.5 mm either side of the T8 lesion epicentre) from both species was isolated, post-fixed for 2 hr in PFA, cryoprotected through a graded series of sucrose solutions and embedded in OCT mounting compound (TAAB Laboratories).

In the first experiment, 6 animals/time-point were killed at 0, 2, 8 and 15 days post-lesion (dpl), to investigate lesion cavity development after injury. This study established that maximal differences in lesion cavity dimensions in rats and mice had developed at 8 dpl. Thus, further rats and mice were used to analyse the injury response at 8dpl in more detail by immunohistochemistry and western blotting.

Haematoxylin and Eosin staining (H+E)

Longitudinal/parasagittal 15 µm-thick sections of the cord through the lesion site were cut using a cryostat (Bright Instruments, Cambridgeshire, UK) and adhered

onto Superfrost Plus Slides (Fisher Scientific, Loughborough, UK). Sections were washed twice in PBS, immersed in Harris's Haematoxylin (BDH, Poole, UK) for 5 min and washed in tap water. Sections were then immersed in Eosin (BDH) for 1 min, washed in tap water, dehydrated through a graded series of alcohols and cleared using 2 changes of Histoclear (National Diagnostics, Atlanta, USA) for 1 and 3 min, respectively. Coverslips were mounted in Vectamount (Vector Laboratories, Peterborough, UK), viewed under a Zeiss Axioplan 2 light microscope and images captured using an Axiocam HRc run from Axiovision 4 software (all from Zeiss, Hertfordshire, UK).

Immunohistochemistry

Sections that contained only the lesion area were thawed for 30 min at room temperature and before proceeding with immunohistochemistry; a second investigator blinded the identity of each section. Randomised sections were then washed twice in PBS, permeabilised in 0.1% Triton X-100 in PBS for 10 min and then washed three times in PBS before blocking non-specific binding with PBS containing 3% BSA (Sigma) and 0.5% Tween 20 (Sigma) for 30 min at room temperature (RT). Sections were incubated with the appropriate primary antibody (Table 1), diluted in blocking solution and incubated overnight at 4ºC in a humidifier chamber for 16-18hr. Sections were then washed three times in PBS and incubated in Alexa488 (green) or Alexa 594 (Red) (Molecular Probes, Oregon, USA) labelled secondary antibodies (Table 1) diluted in blocking solution for 1 hr at RT. Finally, sections were washed three times in PBS, mounted in Vectashield containing DAPI (Vector Labs) and images captured by an Axiocam HRc, using Axiovision 4 software (all from Zeiss). Negative antibody controls (primary antibody omitted) were included

in each run and used to set the background threshold intensity for each antibody and each species.

Protein extraction and western blotting

Six intact controls and 6 DC injured rats/mice were killed at 8 dpl by intraperitoneal injection of Euthatol (Sigma). The T8 lesion site was isolated (lesion site + 3 mm of cord either side of the lesion epicentre for rats and 2 mm either side of the lesion epicentre for mice were removed and immediately snap frozen in liquid nitrogen. To determine the levels of wound healing/angiogenic proteins in mice and rat SCI, tissues were homogenised in ice-cold lysis buffer (1M Tris HCL; pH 7.4, 5M NaCl, 0.5M EDTA, 0.25M EGTA, 1% NP-40 (Sigma)) containing protease inhibitor cocktail (Sigma) and clarified by centrifugation at 13,000 x g for 30 min at 4ºC. Protein concentration was normalised using a calorimetric protein assay according to the manufacturer's instructions (Bio-Rad, Hertfordshire, UK). Total protein (40µg) from each sample was mixed with 2 x Lammelli buffer (Sigma), boiled for 4 min and loaded onto pre-prepared 12% Tris-glycine SDS-PAGE gels. Resolved proteins were transferred onto Immobilon-P polyvinylidene fluoride (PVDF) membranes (Millipore, MA, USA) and blocked in 5% non-fat milk solution for 30 min before incubation with the same primary antibodies as used for immunohistochemistry (Table 1) overnight at 4℃ with constant agitation. Membranes were washed three times in Tris-buffered saline containing Tween 20 (TBST) before incubation with the appropriate HRP-conjugated secondary antibodies (Table 1) for 1hr at RT. Protein bands were detected using an enhanced chemiluminescence (ECL) system according to the manufacturer's instructions (GE Healthcare). Membranes were stripped in a low pH

stripping buffer (25mM glycine-HCl, pH2, 1% SDS (Sigma)) and re-probed as required.

Bands of interest detected by western blot were quantified using densitometry after scanning membranes into Photoshop (keeping scanning parameters the same for all blots), and analysed using the built-in gel plotting macros in ImageJ (NIH, USA). Since antibody cross specificities may vary between mouse and rat tissue, we first normalised densitometric values to those obtained with intact controls from each species and then three separate blots from three independent experiments were also normalised to α-tubulin loading control densities for each species. The results are then presented as mean ± SEM.

Image analysis

Prior to image analysis, the identity of each section was blinded and randomised by a second investigator. To eliminate sample bias caused by the variation in the size of the wound cavity in sections at different wound depths and the relative sizes of rats and mice, cavity sizes from sections taken at similar depths in each animal were compared and quantified

Lesion cavity area. Although sections throughout the lesion cavity were stained to measure the lesion cavity area (Fig. 1), the middle three sections through each lesion cavity, determined by cutting sections from the start to the end of the DC lesion (n = 6 rats/mice/time-point) was used to measure lesion cavity area using ImagePro Analyzer.

Relative fluorescent staining intensity. All photomicrographs were taken at x 5 magnification with the Zeiss Axioplan 2 fluorescent microscope using the same standardised exposure settings throughout for each antibody. Controls from each species where primary antibody was omitted were used to set the background threshold for each species. The middle three sections through each cavity was used to record positive immunostaining for each antibody in pixel counts from a set area of 1.335µm x 1.335µm that included the lesion site. Using ImageJ (NIH, USA), images were thresholded and the mean integrated intensity of pixels/unit area for each antibody was recorded.

Quantification of spared axon density in the dorsal funiculus. Photomicrographs of the dorsal funiculus were captured using the Zeiss Axioplan 2 fluorescent microscope as described above. Using ImageJ (NIH) the relative intensity of $NF200^{+}$ staining was measured in the traced area of the entire dorsal funiculus after normalisation of the background intensity, obtained with omission of primary antibody controls for each species, was subtracted from the positive intensity value. Automatic thresholding for each image using ImageJ was performed to determine the threshold for specific immunoreactivity and pixel intensities above threshold levels were recorded.

Functional test procedures

Thermal sensitivity. Using established methods of Plantar heat sensitivity tests described previously (Detloff et al., 2012; Hargreaves et al., 1988; Lindsey et al., 2000), animals were acclimatised 1-wk before surgery and on -1, 0 (2hr after surgery), 7, 14, 21 and 28 dpl data were collected at the same time of day to ensure

consistency (n = 12 rats/mice (6 sham, 6 DC injured)). Animals were acclimatised in clear Perspex compartments (230mm x 170mm) for 5 min before testing commenced. Once the plantar surface of the hind limbs was placed on the glass with weight support and the animal was stationary, the infra-red (IR) heat source (Harvard Apparatus, Massachusetts, USA) was placed directly beneath the centre of the plantar surface and the beam activated to produce a thermal stimulus to start the trial. The reaction time of paw withdrawal was recorded for 5 separate tests for each hind limb with a 30s interval before re-testing on the same paw. The middle three scores for the hind limbs were averaged to produce a single score for each animal and presented as mean ± SEM.

Mechanical allodynia. To quantify mechanical sensitivity, hindlimb withdrawal responses were quantified using Von Frey hair filament tests. Animals were placed in the Perspex compartment, supplied with food for distraction and allowed to acclimatise for 10 min. Monofilaments representing specific gram weight forces (Stoelting Europe, Dublin) were applied to the plantar surface of each hind paw between the foot pads (previously marked with permanent marker) for a 1-2s period in a steady manner. A withdrawal response of the hind limb to the particular monofilament was recorded as a positive response, while a failure to elicit a withdrawal response was recorded as negative. A total of 10 separate trial responses were recorded for each hind limb with a 30s interval between each recording. Monofilament scores from both hind limbs were averaged to the lowest monofilament level used at which 50% or more trials were positive and converted to gram force and presented as mean ± SEM.

Statistical analysis

Means ± SEM were determined and all statistical comparisons were made in SPSS (IBM) using a one-way analysis of variance (ANOVA) assuming unequal variances followed by post-hoc testing with Dunnett's method to test for statistical differences.

RESULTS

Characterisation of the DC scarring response to injury

$GFAP^+$ astrocytes were abundant in the neuropil, about the lesion site and invading the lesion core in mice (arrows; Fig. 2A and inset). In rats, fewer $GFAP^+$ astrocytes were localised within the lesion and none were seen in the lesion core (Fig. 2B and inset). $Fibronectin^+$ ECM material filled the lesion core in mice (Fig. 2C and inset), whereas little or none was present in rat SCI wounds (Fig. 2D and inset). Low numbers of $CD68^+$ cells were present in both mice (Fig. 2E and inset) and rats (Fig. 2F and inset), and low levels of NG2 were also present in the SCI wounds of both species.

Acute cavity development

Little or no difference in gross anatomy was observed in intact mouse and rat T8 spinal cord segments (Fig. 3A and B). At 2 dpl, there was disruption to the normal architecture of the cord in the two species (Fig. 3C and D), and in rats a lesion cavity had begun to develop (Fig. 3D). Differences between mice and rat DC lesion sites were more obvious at 8 dpl, with tissue disruption in the cord in mice (Fig. 3E) and the development of an obvious wound cavity in rats filled with haematogenous cells,

debris, fibrous material interspersed with small empty cavity areas (Fig. 3F). Both type I and II cavities were present in rat cords at 8 dpl. By 15 dpl, scar tissue had formed at the SCI site but no lesion cavities had developed in mouse cords (Fig. 3G) while, in rats the wound had expanded both rostrally and caudally and contained Type I cavities consisting haematogenous cells (Fig. 3H).

Mean wound cavity area in the rat was 21 x 10^4 ± 7.5 x 10^4 µm² and 26 x 10^4 ± 4 x 10^4 µm² at 8 and 15 dpl, respectively (Fig. 3I). These results confirm that wound cavitation is extensive in the rat cord after DC lesion while in the mouse cavities do not develop.

Laminin deposition in DC lesions

In the intact cord, meningeal and vascular basal laminae were laminin$^+$ in both mice and rats (Fig. 4A and B). At 2 dpl, the levels of laminin deposition did not change significantly, compared to that observed at 0 dpl in both species (Fig. 4C and D), but was enhanced in mice compared to rats in the glia limitans externa (GLE), vascular basal lamina, ECM filled lesion core, lining of Type I cavities and the glia limitans accessoria (GLA) at 8 dpl (Fig. 4E and F). Enhanced levels of laminin$^+$ immunoreactivity in the GLE, basal lamina of the blood vessels, ECM of the lesion core and the GLA remained in 15 dpl mouse lesions (Fig. 4G). In rats at 15dpl, laminin$^+$ immunoreactivity was primarily associated with the GLE and GLA (Fig. 4H), while the laminin$^+$ immunoreactivity did not change significantly in the GLE of both mouse and rat.

Quantification of laminin immunoreactivity reflected these changes, demonstrating significantly enhanced levels of laminin in DC wounds in mice compared to rats at 8 dpl (16 x10^4 ± 5.5 x 10^4 in mice compared to 10 x 10^4 ± 4.0 x

10^4 pixels in rats, P<0.0001) and 15 dpl (14 x 10^4 ± 1.6 x 10^4 in mice compared to 11 x 10^4 ± 2.1 x 10^4 pixels in rats, P<0.0001) (Fig. 4I). These results demonstrate that in mice compared to rats, SCI sites have greater neovascularisation, do not cavitate and have higher levels of ECM molecules.

Comparison of factors in rat and mouse DC wounds at 8 dpl

Since our results thus far demonstrated the greatest differences in cavitation and laminin immunoreactivity at 8 dpl, we selected this time point for further analysis detailed below.

1. Angiogenic growth factors. VEGF-A (Fig. 5A-C, Table 2), TGFβ-2, PDGF-BB, FGF2, angiogenin and angiopoeitin-1 (Table 2) were all significantly higher in mouse SCI sites compared to rats. In the mouse, these growth factors were immunohistochemically localised within the lesion site and surrounding neuropil and up to 5 mm either side of the lesion epicentre (Fig. 5A), whereas in rats they were absent from the lesion site with low levels of immunohistochemistry in the surrounding neuropil.

Western blotting and subsequent densitometry demonstrated that VEGF-A (Fig. 5D, Table 3) and TGF-β2, PDGF-BB, FGF2, angiogenin and angiopoeitin-1 (Table 3) levels were significantly higher in mice compared to rats.

2. MMP and TIMP. MMP-1 (Fig. 6A-C, Table 4), MMP-2 and MMP-9 immunoreactivity (Table 4) were significantly higher in mouse lesion sites compared to the rat and similarly distributed in the lesion site and the surrounding neuropil.

Western blot densitometry of MMP showed that MMP-1 (Fig. 6D and E, Table 5), MMP-2 and MMP-9 levels (Table 5) were greater in mouse lesion sites compared

to rats. In contrast, TIMP-2 immunohistochemical (Fig. 7A-C, Table 4) and western blot (Fig. 7D and E, Table 5) levels were low in mouse lesion sites compared to the rat, with immunoreactivity distributed in the surrounding neuropil of the rat cord but absent in the wound cavity.

3. ECM/scarring-related molecules. Sema-3A immunoreactivity was absent in mice and was high in rat lesion cavities and the peri-lesion neuropil (Fig. 8A-C, Table 6). Conversely, collagen-1 immunoreactivity was highly upregulated in the mouse compared to rat lesion sites (Table 6) and its distribution mirrored that of laminin, i.e. within the lesion in mice and localised to the GLA in the rat (not shown). The cell adhesion molecule, PECAM-1, was also significantly higher in mice compared to rat SCI wounds (Table 6), localised to the lesion site and peri-lesion neuropil (not shown). Western blotting and densitometry confirmed that Sema-3A (Fig. 8D and E, Table 7) and PECAM1 (Table 7) levels were significantly higher in rats compared to mice.

These results demonstrate fundamental differences in healing of SCI wounds in mice compared to rats, i.e. aggressive wound healing in mice marked by increased deposition of matrix proteins, pro-angiogenic growth factors correlated with raised levels of MMP and reduced TIMP titres.

Changes in carbonic anhydrase-X after SCI

CA10 immunoreactivity was seen in the lesion site and peri-lesion neuropil in mice and rats (Fig. 9A and B). At 8 dpl, there was significantly higher levels of CA10 in rats compared to mice (5.6 x10² ± 2.5 x 10^2 pixels in rats compared to -7.6 x 10^2 ± 1.6 x 10^2 pixels in mice, $P<0.001$, Fig. 9C). These results were confirmed by western

blot, demonstrating that the protein levels of CA10 were significantly higher in rat compared to mouse DC lesions (5.5 x10^4 ± 2.0 x 10^4 pixels in rat compared to -5.5 x 10^4 ± 1.8 x 10^6 in mice, P<0.021, Fig. 9D and E). These results show that increased levels of CA10 are observed after DC injury in rats.

Greater sparing of NF200$^+$ DC axons in mice compared to rats

Spared axons in the DC of mice and rats after injury were assessed by calculating the area occupied by NF200 labelling in the whole dorsal funiculus (Bouhy et al., 2011). In spinal segments T7 (above lesion) and T9 (below lesion), normal basal levels of NF200$^+$ Immunostaining was observed in control mice (Fig. 10A and B, respectively) and rats (Fig. 10E and F, respectively), in the CST and in interneurons and their axons in the superficial dorsal horn. After DC injury in mice, NF200 immunohistochemistry was significantly reduced in the CST at T7 and T9 compared to intact controls, indicative of retrograde axonal dyeback of axons that originate from the motor cortex, respectively (Fig. 10C and D). In rat lesioned DC, reduced NF200 immunohistochemistry was observed in spinal segments in the CST from T7 and T9 (Fig. 10G and H), compared to control rats. The reduction in NF200 immunoreactivity in the DC was greater in rat T7 (65 ± 4% in rat *versus* 42 ± 3% in mice, P<0.01) and T9 (45 ± 3% in mice *versus* 20 ± 4% in rat, P<0.01) segments (Fig. 10I) compared to mice.

Similar changes in PKC-γ immunostaining were also observed in DC injured dorsal funiculus of mice and rats (not shown). PKC-γ is an isotope of the classical PKC subfamily, which is solely expressed in the brain and spinal cord and localisation is restricted to neurons (Saito and Shirai, 2002). This restriction allows

determination of axonal sparing after sub-acute DC between mice and rats (Barritt et al., 2006).

Behavioural analysis

The response to thermal stimuli in both rats and mice were significantly impaired 2 hr after DC injury compared to sham-treated control animals (Fig. 11A and B). For example, the reaction time (paw withdrawal latency) was delayed by 3.38s in mice ($P<0.042$) and by 5.63s in rats ($P<0.042$). However, by 7dpl the response to thermal stimuli had returned to sham-treated control levels and showed no further differences in withdrawal latency over the course of the experimental time-period of 28dpl (Fig. 11A and B). Unlike thermal responses, mechanical allodynia responses were not significantly different in mice or rats, with or without DC injury and did not vary over the experimental time-period (not shown). These results indicate that despite the presence of a large wound cavity in rats, DC injury did not affect responses to mechanical stimuli but temporarily affected responses to thermal stimuli in the early stages after DC injury. However, within 7 dpl, animals regained normal function response times and were no different to those observed in sham-treated control animals.

DISCUSSION

We report here that significant differences exist in the acute SCI response in mice compared to rats and that cavitation only develop in rats at early time points. In rats, the wound cavity expands over time and by 15dpl large Type I cavities are present, filled with haematogenous macrophages. In contrast, the mouse lesion site is in-filled

and rich in the ECM molecules laminin and collagen, together with pro-angiogenic and pro-wound healing factors. In addition, levels of axon growth inhibitory Sema-3A and anti-proteolytic TIMP-2 were significantly higher in rat than in mouse SCI sites indicating an environment less conducive to axon growth and wound remodelling. These results support our contention that an enhanced healing response in mice is associated with suppressed cavitation, a response that is facilitated by high levels of pro-angiogenic and pro-wound healing factors. Greater numbers of $NF200^+$ and $PCK\text{-}\gamma^+$ axons were spared in mice compared to rats, suggesting that cavitation is detrimental to axon integrity. Nonetheless, the presence of a large cavity in rats had no effect on mechanical allodynia but thermal allodynia was affected in both mice and rats immediately after injury, recovering to normal levels within 7dpl.

Cavitation

Although small severity-dependent injury cavities have been reported in mouse SCI sites, our results confirm those of others that ECM deposition without cavitation is a more characteristic response (Bilgen et al., 2007; Inman and Steward, 2003). By contrast, rat SCI wounds cavitated by 8dpl and by 15dpl when a large Type I cavity had formed which extended rostrally and caudally from the injury epicentre, filled with haematogenous macrophages and cellular debris. Cavities may develop after vascular regression and endothelial cell loss (Casella et al., 2006; Loy et al., 2002) and their expansion may be exacerbated by hypoxia, necrosis, apoptosis and increased vascular permeability (disruption of the blood spinal cord barrier (BSCB)). Demyelination and neuronal degeneration occur in the surrounding neuropil as the cavity expands (Berry et al., 2008; Blight, 2000; Casella et al., 2006; Fassbender et al., 2011; Hunt et al., 2002; Mautes et al., 2000; Sandvig et al., 2004; Whetstone et

al., 2003). Cavities may expand as damaged tissues are removed by inflammatory macrophages and microglia, explaining the beneficial effects of immunosuppressive therapies which probably maintain structural and functional integrity of the spinal cord (Blight, 1994; Giulian and Robertson, 1990; Guth et al., 1994; Popovich et al., 1999).

Cavitation in the human condition of post-traumatic syringomyelia is a potentially disastrous complication of SCI, causing intractable pain and loss of upper extremity function, and may be life-threatening if the syrinx extends rostrally into the brainstem (Biyani and el Masry, 1994; Edgar and Quail, 1994). Currently, there is no cure for this condition and therefore understanding the differential factors regulating cavitation in mice and rats may lead to the development of potential therapies for this debilitating condition.

Inflammatory responses

Although Sroga et al (2003) reported similar responses of macrophages and microglia in mouse and rat SCI sites, accumulation of T-cells at the wound peaks in rats between 3 and 7dpl and declines by 50% over the next three weeks, while T-cell entry is not evident in the mouse until after 14dpl (Sroga et al., 2003). Dendritic cells (normally absent in control rat and mouse spinal cords) infiltrate SCI wounds with T-cells in rats but not in mice, suggesting another species difference in inflammatory reactions to SCI (Sroga et al., 2003). Antigen-presenting dendritic cells can both activate or kill T-cell (Bernstein et al., 1986) and their accumulation in a SCI wound could be detrimental by stimulating infiltration of T-cells into the cord, or protective by removing cytotoxic T-cells. Furthermore, cells resembling lymphocytes but not expressing lymphocyte markers, a phenotype characteristic of fibrocytes, which are

specialised blood-borne cells, involved in wound healing and immunity, are also present only in mice (Chesney and Bucala, 1997; Sroga et al., 2003). Although these differential inflammatory responses may explain why mice do not cavitate, it remains to be determined whether they contribute to the different injury responsive molecular profiles observed between the two species.

Angiogenic growth factors

Angiogenesis is beneficial in reducing secondary axonal damage after SCI, protecting against ischemia by increasing oxygen delivery and nutrients to sites of regeneration and removal of metabolic waste (Loy et al., 2002; Lutton et al., 2012). After traumatic SCI in the two species, blood vessels fracture leading to disruption of the blood-spinal cord barrier (BSCB) and exposure of the neuopil to the damaging effects of inflammatory macrophages and microglia (Noble and Wrathall, 1985; Schlosshauer, 1993). Our mouse SCI wounds were filled with pro-angiogenic/pro-wound healing factors that were largely absent from rat lesion sites. The higher levels of laminin and collagen in mouse lesion sites after SCI provide essential matrix scaffolds (Okada et al., 2007) for angiogenesis and tissue remodelling, which promote better wound healing properties. The expression of several potent angiogenic factors were more positively modulated in the injured mouse *versus* rat cord, including VEGF-A, angiogenic, and this was reflected by a more robust angiogenic response. Other factors important to the healing process were also higher in mouse compared to rat SCI wounds. For example, FGF2, which exerts neurotrophic and neurite outgrowth properties in culture (Moftah, 2007) also contributes to wound healing (Carmeliet and Jain, 2000; Chung and Ferrara, 2010; Hiraoka et al., 1998).

The high levels of PECAM1 in mouse SCI wounds may promote angiogenesis (Newman, 1997) and also remove aged neutrophils, aiding in leukocyte migration and activating integrins, thereby contributing to wound-healing and revascularisation after injury (Goussev et al., 2003; Newman, 1997; Whetstone et al., 2003). Angiopoietin-1 induces PECAM1 and tight junction proteins such as occludin and ZO-2 which restore BSCB integrity by limiting vascular permeability (Gamble et al., 2000; Hori et al., 2004; Lee et al., 2009), strengthening paracellular interactions and reducing the number and size of endothelial gap junctions (Baffert et al., 2006; Wong et al., 1997). Angiogenin on the other hand, has definitive neuroprotective properties on motor neurons (Kieran et al., 2008), and may provide similar neuroprotection in our SCI wounds. VEGF is also likely to contribute to better wound healing in the mouse since it modulates inflammatory reactions, creating a microenvironment that contributes to axon preservation and sprouting through maturation, stability and wound healing properties (Chung and Ferrara, 2010; Khalil et al., 1989; Lutton et al., 2012).

MMP and TIMP

Enhanced levels of MMP-2 and MMP-9 are detectable in the acute phase after SCI, facilitating inflammatory cell infiltration and permeability of BSCB (Biddison et al., 1997; Delclaux et al., 1996; Gronski et al., 1997; Rosenberg, 1995). Thus, treatment with either MMP inhibitors or neutralizing antibodies to MMP can protect against BSCB breakdown and prevent inflammatory cell infiltration (Romanic et al., 1998; Rosenberg, 1995). The high levels of MMP and low levels of TIMP observed here in the mouse SCI wounds is thought to be conducive to wound healing since MMP-1, -2 and -9 are all required during angiogenesis and are detected at high levels in sites

of angiogenesis (Hiraoka et al., 1998; Iwasaka et al., 1996; Zucker et al., 1995). MMP-mediated proteolysis thus facilitates invasion of endothelial cells into the wound matrix, generates ECM degradation products that are chemotactic for endothelial cells and releases ECM bound growth factors to aid the healing process.

Hypoxia and angiogenesis

Although hypoxia regulates angiogenesis (Potter and Harris, 2004), the higher levels of carbonic anhydrase observed in rats in our experiments did not correlate with this assertion. Despite CNS expression of CA10 (Okamoto et al., 2001; Taniuchi et al., 2002), other isoforms of carbonic anhydrase contribute to neuronal death and blood-brain barrier (BBB) disruption after brain and retinal injury (Gao et al., 2007; Guo et al., 2012). Higher CA10 levels seen in the rat may, therefore, act similarly causing an increase in BBB permeability, neuronal death and oedema, all of which are detrimental to recovery from SCI.

Semaphorin-3A

We found raised levels of Sema-3A in and around the lesion site after SCI in rats while Sema-3A was almost completely absent in mouse suggesting that Sema-3A deposition hinders wound healing and contributes to the cavity development. Sema-3A has multiple functions including blocking axon regeneration after binding to its co-receptor; NP1 on axonal growth cones (Schlomann et al., 2009; Shelly et al., 2011), while inhibition of Sema-3A is a potential therapeutic treatment for promoting axon regeneration after SCI (Kaneko et al., 2006; Mire et al., 2008). In addition, Sema-3A binds VEGF and its plexin receptors and directs angiogenesis (Neufeld et al., 2005; Soker et al., 2002; Tamagnone et al., 1999).

Axonal sparing and behavioural testing

Our assumptions that axonal sparing would be enhanced in mice due to the lack of cavitation was borne out by the observation of the significantly lower reduction in PKC-γ immunoreactivity seen in the mouse compared to the rat CST spinal segments above and below the lesion. These results suggest that axonal dieback and Wallerian degeneration are increased in rats compared to mice and may be caused by the extension of the cavity both rostrally and caudally in rat SCI sites. However, reductions in PKC-γ immunoreactivity indicating relative axon sparing in the mouse, did not correlate with behavioural deficits in injured animals assessed using IR heat and Vonfrey hair filament tests. Hill et al (2009) demonstrated using a LISA-Vibraknife that generates precise dorsal lacerations, that injury depths between 0.5-1.0mm did not affect behavioural tests similar to those used in our study (Hill et al., 2009). However, since detrimental effects were only observed beyond a DC lesion depth of 1.1mm, lesions deeper than 0.8mm may be required to obtain behavioural deficits after DC injury. However, other studies using weight drop devices that produce more overt injuries than DC crush have shown that lesion severity correlates with the extent of behavioural deficits in mouse SCI models (Farooque, 2000; Ma et al., 2001; Seki et al., 2002).

Although we have used an inbred mouse (C57Bl6) and outbred rat (Sprague-Dawley) strain to investigate cavitation, equivalent responses to DC injury have been observed in other outbred rat strains such as Long Evans and Wistar rats (Jimenez et al., 2005; Byrnes et al., 2010; Schwartz et a., 1999; Poon et al., 2007; Lagord et al., 2002; Figley et al., 2014) as well as inbred strains such as Lewis rats (Sroga et al., 2003). The extent of cavitation however, is dependent on the severity of the initial injury (Poon et al., 2007). Furthermore, there is no consistency across inbred and

outbred strain to indicate that cavitation would be different in one group of animals versus the other group. For example, SCI in inbred and outbred strains of mice that are either resistant or susceptible to excitotoxicity all showed increases in lesion size over the first 7 days followed by decreases in cavity size and wound-healing from 7 to 56 days, although animals susceptible to excitotoxicity showed larger lesion sizes across all strains (Inman et al., 2002). Therefore, our results are valid across a range of rat and mouse strains and highlights the differences in cavity formation, matrix deposition and wound healing responses.

Conclusion

In conclusion, differences do exist between mice and rats in cavity formation, matrix deposition and pro-angiogenic protein levels after DC injury, indicating that mice have a more robust angiogenic and wound healing response to SCI that is associated with less cavitation and resultant axon sparing. Despite losses in PKC-γ immunoreactivity in DC above and below the lesion in both species, only the response to thermal stimuli was reduced 2 hr after injury with response times returning to normal within 7 dpl compared to sham controls in mice and rats. Our results support the hypothesis that the absence of cavitation in mice is due to an adequate balance between angiogenesis, wound healing and scar deposition compared to rats that fail to lay down ECM after sub-acute SCI. Our results indicate key differences between the wound healing response in mice compared to rats that requires further investigation.

ACKNOWLEDGEMENTS

This work was supported by a BBSRC Doctoral Training Grant (grant no. BB/F017553/1).

FIGURE LEGENDS

Fig. 1. Area of acute DC wound cavity at increasing depths from the surface of the spinal cord (n = 6 rats represented by different symbols shown in the key). Three sections chosen at different depths through the lesion were immunostained for laminin and GFAP and used to measure the size of the cavity in 6 different animals in the rat.

Fig. 2. Acute SCI response in mice and rats. Immunohistochemistry to show changes in GFAP (A and B), fibronectin (C and D), CD68 (E and F) and NG2 (G and H) at 8 dpl within and about DC lesions (* = lesion epicentre; scale bars in A-H = 200 μm; arrows in A = $GFAP^+$ astrocytes invading the lesion core; A-D and E-H are consecutive sections, respectively).

Fig. 3. Histological differences in wound cavitation in mice and rats at 0 (A and B), 2 (C and D), 8 (E and F) and 15 dpl (G and H). Rat lesion cavity area determined by haematoxylin and eosin staining of the middle section of each cavity between 0-15dpl (I) (n = 6/group/time-point; * = lesion epicentre; scale bars in A-I = 200 μm; arrowheads in D, F and H = cell free areas in rat SCI cavities).

Fig. 4. Localisation of laminin in the lesion site over the 15 dpl time in DC lesions in mice and rats. Expression of laminin in intact controls (A and B) and at 2 (C and D), 8 (E and F) and 15 dpl (G and H). Pixel intensities were calculated and average pixel counts were plotted showing significant differences in laminin expression between mice and rats (I) (n = 5/group/time-point; * = lesion epicentre; scale bars in A-H = 200 µm; arrowheads = glia limitans externa (GLE); arrows = glia limitans accessoria (GLA); open arrows = blood vessels).

Fig. 5. The localisation of VEGF-A at 8 dpl in DC lesions. Immunohistochemistry for VEGF-A in mice (A) and in rats (B) and the pixel intensities of VEGF-A^+ fluorescence (C). Western blot (D) and densitometry (E) corroborated the immunohistochemistry results (α-tubulin was used as a protein loading control (F); scale bars in A and B = 200 µm).

Fig. 6. The localisation of MMP-1 at 8 dpl after DC lesion. Immunohistochemistry for MMP-1 in mouse (A) and rat (B) and the pixel intensities of MMP-1^+ fluorescence (C). Western blot (D) and densitometry (E) was used to corroborate the immunohistochemistry results (the same α-tubulin was used as a protein loading control as in Figure 4F; scale bars in A and B = 200 µm).

Fig. 7. The localisation of TIMP-2 at 8 dpl in DC lesions. Immunohistochemistry for TIMP-2 in mouse (A) and rat (B) and the pixel intensities of TIMP-2^+ fluorescence (C). Western blot (D) and densitometry (E) corroborated the immunohistochemistry results (the same α-tubulin was used as a protein loading control as in Figure 4F; scale bars in A and B = 200 µm).

Fig. 8. The localisation of Sema-3A at 8 dpl in DC lesions. Immunohistochemistry for Sema-3A in mouse (A) and rat (B) and the pixel intensities of Sema-3A$^+$ fluorescence (C). Western blot (D) and densitometry (E) corroborate the immunohistochemistry results (the same α-tubulin was used as a protein loading control as Figure 4F; scale bars in A and B = 200 μm).

Fig. 9. The localisation of CA9, a marker of hypoxia after DC lesion at 8 dpl in mice and rats. (A) and (B) immunohistochemistry and (C) quantification of the CA9$^+$ pixel intensities in the lesion site and peri-lesion neuropil in mice and rats. (D) Western blot and (E) densitometry from tissue lysates to demonstrate proteins levels of CA9 in the DC lesion of mice and rats (scale bars in A and B = 200μm).

Fig. 10. NF200 immunoreactivity as an indicator of axonal sparing at 8dpl after DC injury in spinal segments above and below the lesion. Representative NF200 staining at T7 (above lesion) in mouse control (A) and injured (C) and at T9 control (B) and injured (D) cords. Representative NF200 staining at T7 in rat control (E) and injured (G) and at T9 control (F) and injured (H) cords. Quantification of the immunoreactivity (I) demonstrated that NF200 immunoreactivity was reduced in rats compared to mice at both T7 and T9 spinal segments. Scale bars = 200 μm. Diagram shows dorsal column and corticospinal tract axons quantified in (I).

Fig. 11. Comparison of the behavioural deficits observed after T8 DC injury in mice and rats over time using IR plantar heat test. Quantification on the average reaction time before surgery (-1), 2 hours after surgery (0), 7, 14, 21 and 28 dpl showed significant differences in mice (A) and rats (B) at 0dpl only compared to control.

References

Ahmed, Z., Read, M.L., Berry, M., Logan, A., 2010. Satellite glia not DRG neurons constitutively activate EGFR but EGFR inactivation is not correlated with axon regeneration. Neurobiol Dis 39, 292-300.

Baffert, F., Le, T., Thurston, G., McDonald, D.M., 2006. Angiopoietin-1 decreases plasma leakage by reducing number and size of endothelial gaps in venules. Am J Physiol-Heart C 290, H107-H118.

Barritt, A.W., Davies, M., Marchand, F., Hartley, R., Grist, J., Yip, P., McMahon, S.B., Bradbury, E.J., 2006. Chondroitinase ABC promotes sprouting of intact and injured spinal systems after spinal cord injury. J Neurosci 26, 10856-10867.

Bazley, F.A., Hu, C., Maybhate, A., Pourmorteza, A., Pashai, N., Thakor, N.V., Kerr, C.L., All, A.H., 2012. Electrophysiological evaluation of sensory and motor pathways after incomplete unilateral spinal cord contusion. J Neurosurg Spine 16, 414-423.

Benton, R.L., Maddie, M.A., Gruenthal, M.J., Hagg, T., Whittemore, S.R., 2009. Neutralizing endogenous VEGF following traumatic spinal cord injury modulates microvascular plasticity but not tissue sparing or functional recovery. Curr Neurovasc Res 6, 124-131.

Benton, R.L., Whittemore, S.R., 2003. VEGF165 therapy exacerbates secondary damage following spinal cord injury. Neurochem Res 28, 1693-1703.

Bernstein, R.M., Morgan, S.H., Bunn, C.C., Gainey, R.C., Hughes, G.R., Mathews, M.B., 1986. The SL autoantibody-antigen system: clinical and biochemical studies. Ann Rheum Dis 45, 353-358.

Berry, M., Ahmed, Z., Lorber, B., Douglas, M., Logan, A., 2008. Regeneration of axons in the visual system. Restor Neurol Neurosci 26, 147-174.

Biddison, W.E., Taub, D.D., Cruikshank, W.W., Center, D.M., Connor, E.W., Honma, K., 1997. Chemokine and matrix metalloproteinase secretion by myelin proteolipid protein-specific CD8+ T cells: potential roles in inflammation. J Immunol 158, 3046-3053.

Bilgen, M., Al-Hafez, B., Alrefae, T., He, Y.Y., Smirnova, I.V., Aldur, M.M., Festoff, B.W., 2007. Longitudinal magnetic resonance imaging of spinal cord injury in mouse: changes in signal patterns associated with the inflammatory response. Magn Reson Imaging 25, 657-664.

Biyani, A., el Masry, W.S., 1994. Post-traumatic syringomyelia: a review of the literature. Paraplegia 32, 723-731.

Blight, A.R., 1994. Effects of silica on the outcome from experimental spinal cord injury: implication of macrophages in secondary tissue damage. Neuroscience 60, 263-273.

Blight, A.R., 2000. Animal Models Of Spinal Cord Injury. 6, 13.

Bouhy, D., Ghasemlou, N., Lively, S., Redensek, A., Rathmore K.I., Schlichter, L.C., David S. (2011). J Neurosci 31, 16298-16308.

Byrnes, K.R., Fricke, S.T., Faden, A.I., 2010. Neuropathological differences between rats and mice after spinal cord injury. J Magn Reson Imaging 32, 836-846.

Carmeliet, P., Jain, R.K., 2000. Angiogenesis in cancer and other diseases. Nature 407, 249-257.

Casella, G.T., Bunge, M.B., Wood, P.M., 2006. Endothelial cell loss is not a major cause of neuronal and glial cell death following contusion injury of the spinal cord. Exp Neurol 202, 8-20.

Casella, G.T., Marcillo, A., Bunge, M.B., Wood, P.M., 2002. New vascular tissue rapidly replaces neural parenchyma and vessels destroyed by a contusion injury to the rat spinal cord. Exp Neurol 173, 63-76.

Chesney, J., Bucala, R., 1997. Peripheral blood fibrocytes: novel fibroblast-like cells that present antigen and mediate tissue repair. Biochem Soc Trans 25, 520-524.

Chung, A.S., Ferrara, N., 2010. The Extracellular Matrix & Angiogenesis: Role of the Extracellular Matrix in Developing Vessels and Tumor Angiogenesis.

De Laporte, L., des Rieux, A., Tuinstra, H.M., Zelivyanskaya, M.L., De Clerck, N.M., Postnov, A.A., Preat, V., Shea, L.D., 2011. Vascular endothelial growth factor and fibroblast growth factor 2 delivery from spinal cord bridges to enhance angiogenesis following injury. J Biomed Mater Res A 98, 372-382.

Delclaux, C., Delacourt, C., D'Ortho, M.P., Boyer, V., Lafuma, C., Harf, A., 1996. Role of gelatinase B and elastase in human polymorphonuclear neutrophil migration across basement membrane. Am J Respir Cell Mol Biol 14, 288-295.

Detloff, M.R., Fisher, L.C., Deibert, R.J., Basso, D.M., 2012. Acute and chronic tactile sensory testing after spinal cord injury in rats. J Vis Exp, e3247.

Dray, C., Rougon, G., Debarbieux, F., 2009. Quantitative analysis by in vivo imaging of the dynamics of vascular and axonal networks in injured mouse spinal cord. Proc Natl Acad Sci U S A 106, 9459-9464.

Edgar, R., Quail, P., 1994. Progressive post-traumatic cystic and non-cystic myelopathy. Br J Neurosurg 8, 7-22.

Farooque, M., 2000. Spinal cord compression injury in the mouse: presentation of a model including assessment of motor dysfunction. Acta Neuropathol 100, 13-22.

Fassbender, J.M., Whittemore, S.R., Hagg, T., 2011. Targeting microvasculature for neuroprotection after SCI. Neurotherapeutics 8, 240-251.

Figley, S.A., Khosravi, R., Legasto, J.M., Tseng, Y.F., Fehlings, M.G., 2014. Characterization of Vascular Disruption and Blood-Spinal Cord Barrier Permeability following Traumatic Spinal Cord Injury. J Neurotrauma 31, 541-552.

Fitch, M.T., Doller, C., Combs, C.K., Landreth, G.E., Silver, J., 1999. Cellular and molecular mechanisms of glial scarring and progressive cavitation: in vivo and in vitro analysis of inflammation-induced secondary injury after CNS trauma. J Neurosci 19, 8182-8198.

Fujiyoshi, K., Yamada, M., Nakamura, M., Yamane, J., Katoh, H., Kitamura, K., Kawai, K., Okada, S., Momoshima, S., Toyama, Y., Okano, H., 2007. In vivo tracing of neural tracts in the intact and injured spinal cord of marmosets by diffusion tensor tractography. J Neurosci 27, 11991-11998.

Gamble, J.R., Drew, J., Trezise, L., Underwood, A., Parsons, M., Kasminkas, L., Rudge, J., Yancopoulos, G., Vadas, M.A., 2000. Angiopoietin-1 is an antipermeability and anti-inflammatory agent in vitro and targets cell junctions. Circ Res 87, 603-607.

Gao, B.B., Clermont, A., Rook, S., Fonda, S.J., Srinivasan, V.J., Wojtkowski, M., Fujimoto, J.G., Avery, R.L., Arrigg, P.G., Bursell, S.E., Aiello, L.P., Feener, E.P., 2007. Extracellular carbonic anhydrase mediates hemorrhagic retinal and cerebral vascular permeability through prekallikrein activation. Nat Med 13, 181-188.

Giulian, D., Robertson, C., 1990. Inhibition of mononuclear phagocytes reduces ischemic injury in the spinal cord. Ann Neurol 27, 33-42.

Goldshmit, Y., Sztal, T.E., Jusuf, P.R., Hall, T.E., Nguyen-Chi, M., Currie, P.D., 2012. Fgf-dependent glial cell bridges facilitate spinal cord regeneration in zebrafish. J Neurosci 32, 7477-7492.

Goussev, S., Hsu, J.Y., Lin, Y., Tjoa, T., Maida, N., Werb, Z., Noble-Haeusslein, L.J., 2003. Differential temporal expression of matrix metalloproteinases after spinal cord injury: relationship to revascularization and wound healing. J Neurosurg 99, 188-197.

Gronski, T.J., Jr., Martin, R.L., Kobayashi, D.K., Walsh, B.C., Holman, M.C., Huber, M., Van Wart, H.E., Shapiro, S.D., 1997. Hydrolysis of a broad spectrum of extracellular matrix proteins by human macrophage elastase. J Biol Chem 272, 12189-12194.

Guo, F., Hua, Y., Wang, J., Keep, R.F., Xi, G., 2012. Inhibition of carbonic anhydrase reduces brain injury after intracerebral hemorrhage. Transl Stroke Res 3, 130-137.

Guth, L., Zhang, Z., DiProspero, N.A., Joubin, K., Fitch, M.T., 1994. Spinal cord injury in the rat: treatment with bacterial lipopolysaccharide and indomethacin enhances cellular repair and locomotor function. Exp Neurol 126, 76-87.

Han, S., Arnold, S.A., Sithu, S.D., Mahoney, E.T., Geralds, J.T., Tran, P., Benton, R.L., Maddie, M.A., D'Souza, S.E., Whittemore, S.R., Hagg, T., 2010. Rescuing

vasculature with intravenous angiopoietin-1 and alpha v beta 3 integrin peptide is protective after spinal cord injury. Brain 133, 1026-1042.

Hargreaves, K., Dubner, R., Brown, F., Flores, C., Joris, J., 1988. A new and sensitive method for measuring thermal nociception in cutaneous hyperalgesia. Pain 32, 77-88.

He, X., Knepper, M., Ding, C., Li, J., Castro, S., Siddiqui, M., Schachner, M., 2012. Promotion of spinal cord regeneration by neural stem cell-secreted trimerized cell adhesion molecule L1. PLoS One 7, e46223.

Herrera, J.J., Sundberg, L.M., Zentilin, L., Giacca, M., Narayana, P.A., 2010. Sustained expression of vascular endothelial growth factor and angiopoietin-1 improves blood-spinal cord barrier integrity and functional recovery after spinal cord injury. J Neurotrauma 27, 2067-2076.

Hill, R.L., Zhang, Y.P., Burke, D.A., Devries, W.H., Zhang, Y., Magnuson, D.S., Whittemore, S.R., Shields, C.B., 2009. Anatomical and functional outcomes following a precise, graded, dorsal laceration spinal cord injury in C57BL/6 mice. J Neurotrauma 26, 1-15.

Hiraoka, N., Allen, E., Apel, I.J., Gyetko, M.R., Weiss, S.J., 1998. Matrix metalloproteinases regulate neovascularization by acting as pericellular fibrinolysins. Cell 95, 365-377.

Hori, S., Ohtsuki, S., Hosoya, K., Nakashima, E., Terasaki, T., 2004. A pericyte-derived angiopoietin-1 multimeric complex induces occludin gene expression in brain capillary endothelial cells through Tie-2 activation in vitro. J Neurochem 89, 503-513.

Hunt, D., Coffin, R.S., Anderson, P.N., 2002. The Nogo receptor, its ligands and axonal regeneration in the spinal cord; a review. J Neurocytol 31, 93-120.

Inman, D.M., Steward, O., 2003. Physical size does not determine the unique histopathological response seen in the injured mouse spinal cord. J Neurotrauma 20, 33-42.

Iwasaka, C., Tanaka, K., Abe, M., Sato, Y., 1996. Ets-1 regulates angiogenesis by inducing the expression of urokinase-type plasminogen activator and matrix metalloproteinase-1 and the migration of vascular endothelial cells. J Cell Physiol 169, 522-531.

Jimenez Hamann, M.C., Tator, C.H., Shoichet, M.S., 2005. Injectable intrathecal delivery system for localized administration of EGF and FGF-2 to the injured rat spinal cord. Exp Neurol 194, 106-119.

Kaneko, S., Iwanami, A., Nakamura, M., Kishino, A., Kikuchi, K., Shibata, S., Okano, H.J., Ikegami, T., Moriya, A., Konishi, O., Nakayama, C., Kumagai, K., Kimura, T., Sato, Y., Goshima, Y., Taniguchi, M., Ito, M., He, Z., Toyama, Y., Okano, H., 2006. A selective Sema3A inhibitor enhances regenerative responses and functional recovery of the injured spinal cord. Nat Med 12, 1380-1389.

Khalil, N., Bereznay, O., Sporn, M., Greenberg, A.H., 1989. Macrophage production of transforming growth factor beta and fibroblast collagen synthesis in chronic pulmonary inflammation. The Journal of experimental medicine 170, 727-737.

Kieran, D., Sebastia, J., Greenway, M.J., King, M.A., Connaughton, D., Concannon, C.G., Fenner, B., Hardiman, O., Prehn, J.H., 2008. Control of motoneuron survival by angiogenin. J Neurosci 28, 14056-14061.

Kohta, M., Kohmura, E., Yamashita, T., 2009. Inhibition of TGF-beta1 promotes functional recovery after spinal cord injury. Neurosci Res 65, 393-401.

Lagord, C., Berry, M., Logan, A., 2002. Expression of TGFbeta2 but not TGFbeta1 correlates with the deposition of scar tissue in the lesioned spinal cord. Mol Cell Neurosci 20, 69-92.

Lee, S.W., Kim, W.J., Jun, H.O., Choi, Y.K., Kim, K.W., 2009. Angiopoietin-1 reduces vascular endothelial growth factor-induced brain endothelial permeability via upregulation of ZO-2. Int J Mol Med 23, 279-284.

Lindsey, A.E., LoVerso, R.L., Tovar, C.A., Hill, C.E., Beattie, M.S., Bresnahan, J.C., 2000. An analysis of changes in sensory thresholds to mild tactile and cold stimuli after experimental spinal cord injury in the rat. Neurorehabil Neural Repair 14, 287-300.

Loy, D.N., Crawford, C.H., Darnall, J.B., Burke, D.A., Onifer, S.M., Whittemore, S.R., 2002. Temporal progression of angiogenesis and basal lamina deposition after contusive spinal cord injury in the adult rat. J Comp Neurol 445, 308-324.

Lutton, C., Young, Y.W., Williams, R., Meedeniya, A.C., Mackay-Sim, A., Goss, B., 2012. Combined VEGF and PDGF treatment reduces secondary degeneration after spinal cord injury. J Neurotrauma 29, 957-970.

Ma, M., Basso, D.M., Walters, P., Stokes, B.T., Jakeman, L.B., 2001. Behavioral and histological outcomes following graded spinal cord contusion injury in the C57Bl/6 mouse. Exp Neurol 169, 239-254.

Mautes, A.E., Weinzierl, M.R., Donovan, F., Noble, L.J., 2000. Vascular events after spinal cord injury: contribution to secondary pathogenesis. Physical therapy 80, 673-687.

Mire, E., Thomasset, N., Jakeman, L.B., Rougon, G., 2008. Modulating Sema3A signal with a L1 mimetic peptide is not sufficient to promote motor recovery and axon regeneration after spinal cord injury. Mol Cell Neurosci 37, 222-235.

Moftah, M.Z., 2007. Differntial effects of FGF-2 on cell cultures from juvenile brainstem and body spinal cord of the urodele. 48, 21-44.

Neufeld, G., Shraga-Heled, N., Lange, T., Guttmann-Raviv, N., Herzog, Y., Kessler, O., 2005. Semaphorins in cancer. Frontiers in bioscience : a journal and virtual library 10, 751-760.

Newman, P.J., 1997. The biology of PECAM-1. The Journal of clinical investigation 99, 3-8.

Noble, L.J., Wrathall, J.R., 1985. Spinal cord contusion in the rat: morphometric analyses of alterations in the spinal cord. Exp Neurol 88, 135-149.

Nordblom, J., Persson, J.K., Aberg, J., Blom, H., Engqvist, H., Brismar, H., Sjodahl, J., Josephson, A., Frostell, A., Thams, S., Brundin, L., Svensson, M., Mattsson, P., 2012. FGF1 containing biodegradable device with peripheral nerve grafts induces corticospinal tract regeneration and motor evoked potentials after spinal cord resection. Restor Neurol Neurosci 30, 91-102.

Okada, M., Miyamoto, O., Shibuya, S., Zhang, X., Yamamoto, T., Itano, T., 2007. Expression and role of type I collagen in a rat spinal cord contusion injury model. Neurosci Res 58, 371-377.

Okamoto, N., Fujikawa-Adachi, K., Nishimori, I., Taniuchi, K., Onishi, S., 2001. cDNA sequence of human carbonic anhydrase-related protein, CA-RP X: mRNA expressions of CA-RP X and XI in human brain. Biochim Biophys Acta 1518, 311-316.

Oudega, M., 2012. Molecular and cellular mechanisms underlying the role of blood vessels in spinal cord injury and repair. Cell Tissue Res 349, 269-288.

Poon, P.C., Gupta, D., Shoichet, M.S., Tator, C.H., 2007. Clip compression model is useful for thoracic spinal cord injuries: histologic and functional correlates. Spine (Phila Pa 1976) 32, 2853-2859.

Popovich, P.G., Guan, Z., Wei, P., Huitinga, I., van Rooijen, N., Stokes, B.T., 1999. Depletion of hematogenous macrophages promotes partial hindlimb recovery and neuroanatomical repair after experimental spinal cord injury. Exp Neurol 158, 351-365.

Potter, C., Harris, A.L., 2004. Hypoxia inducible carbonic anhydrase IX, marker of tumour hypoxia, survival pathway and therapy target. Cell Cycle 3, 164-167.

Romanic, A.M., White, R.F., Arleth, A.J., Ohlstein, E.H., Barone, F.C., 1998. Matrix metalloproteinase expression increases after cerebral focal ischemia in rats: inhibition of matrix metalloproteinase-9 reduces infarct size. Stroke 29, 1020-1030.

Rosenberg, G.A., 1995. Matrix metalloproteinases in brain injury. J Neurotrauma 12, 833-842.

Saito, N., Shirai, Y., 2002. Protein kinase C gamma (PKC gamma): function of neuron specific isotype. J Biochem 132, 683-687.

Sandvig, A., Berry, M., Barrett, L.B., Butt, A., Logan, A., 2004. Myelin-, reactive glia-, and scar-derived CNS axon growth inhibitors: expression, receptor signaling, and correlation with axon regeneration. Glia 46, 225-251.

Schlomann, U., Schwamborn, J.C., Muller, M., Fassler, R., Puschel, A.W., 2009. The stimulation of dendrite growth by Sema3A requires integrin engagement and focal adhesion kinase. J Cell Sci 122, 2034-2042.

Schlosshauer, B., 1993. The blood-brain barrier: morphology, molecules, and neurothelin. Bioessays 15, 341-346.

Schwartz, E.D., Yezierski, R.P., Pattany, P.M., Quencer, R.M., Weaver, R.G., 1999. Diffusion-weighted MR imaging in a rat model of syringomyelia after excitotoxic spinal cord injury. AJNR Am J Neuroradiol 20, 1422-1428.

Seki, T., Hida, K., Tada, M., Koyanagi, I., Iwasaki, Y., 2002. Graded contusion model of the mouse spinal cord using a pneumatic impact device. Neurosurgery 50, 1075-1081; discussion 1081-1072.

Shelly, M., Cancedda, L., Lim, B.K., Popescu, A.T., Cheng, P.L., Gao, H., Poo, M.M., 2011. Semaphorin3A regulates neuronal polarization by suppressing axon formation and promoting dendrite growth. Neuron 71, 433-446.

Soker, S., Miao, H.-Q., Nomi, M., Takashima, S., Klagsbrun, M., 2002. VEGF165 mediates formation of complexes containing VEGFR-2 and neuropilin-1 that enhance VEGF165-receptor binding. Journal of cellular biochemistry 85, 357-368.

Sroga, J.M., Jones, T.B., Kigerl, K.A., McGaughy, V.M., Popovich, P.G., 2003. Rats and mice exhibit distinct inflammatory reactions after spinal cord injury. J Comp Neurol 462, 223-240.

Sundberg, L.M., Herrera, J.J., Narayana, P.A., 2011. Effect of vascular endothelial growth factor treatment in experimental traumatic spinal cord injury: in vivo longitudinal assessment. J Neurotrauma 28, 565-578.

Tamagnone, L., Artigiani, S., Chen, H., He, Z., Ming, G.I., Song, H., Chedotal, A., Winberg, M.L., Goodman, C.S., Poo, M., Tessier-Lavigne, M., Comoglio, P.M., 1999. Plexins are a large family of receptors for transmembrane, secreted, and GPI-anchored semaphorins in vertebrates. Cell 99, 71-80.

Taniuchi, K., Nishimori, I., Takeuchi, T., Fujikawa-Adachi, K., Ohtsuki, Y., Onishi, S., 2002. Developmental expression of carbonic anhydrase-related proteins VIII, X, and XI in the human brain. Neuroscience 112, 93-99.

Whetstone, W.D., Hsu, J.Y., Eisenberg, M., Werb, Z., Noble-Haeusslein, L.J., 2003. Blood-spinal cord barrier after spinal cord injury: relation to revascularization and wound healing. J Neurosci Res 74, 227-239.

Widenfalk, J., Lipson, A., Jubran, M., Hofstetter, C., Ebendal, T., Cao, Y., Olson, L., 2003. Vascular endothelial growth factor improves functional outcome and decreases secondary degeneration in experimental spinal cord contusion injury. Neuroscience 120, 951-960.

Wong, A.L., Haroon, Z.A., Werner, S., Dewhirst, M.W., Greenberg, C.S., Peters, K.G., 1997. Tie2 expression and phosphorylation in angiogenic and quiescent adult tissues. Circ Res 81, 567-574.

Zucker, S., Lysik, R.M., DiMassimo, B.I., Zarrabi, H.M., Moll, U.M., Grimson, R., Tickle, S.P., Docherty, A.J., 1995. Plasma assay of gelatinase B: tissue inhibitor of metalloproteinase complexes in cancer. Cancer 76, 700-708.

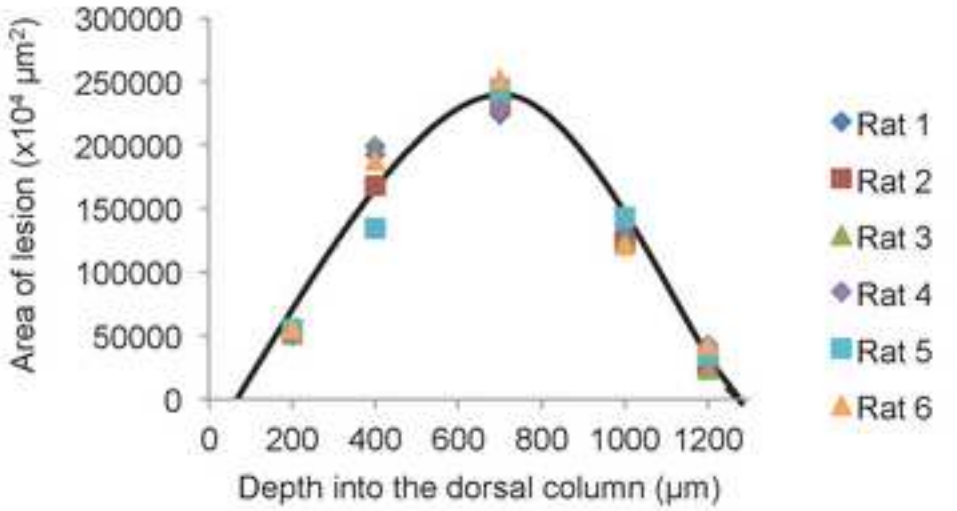

Figure 1

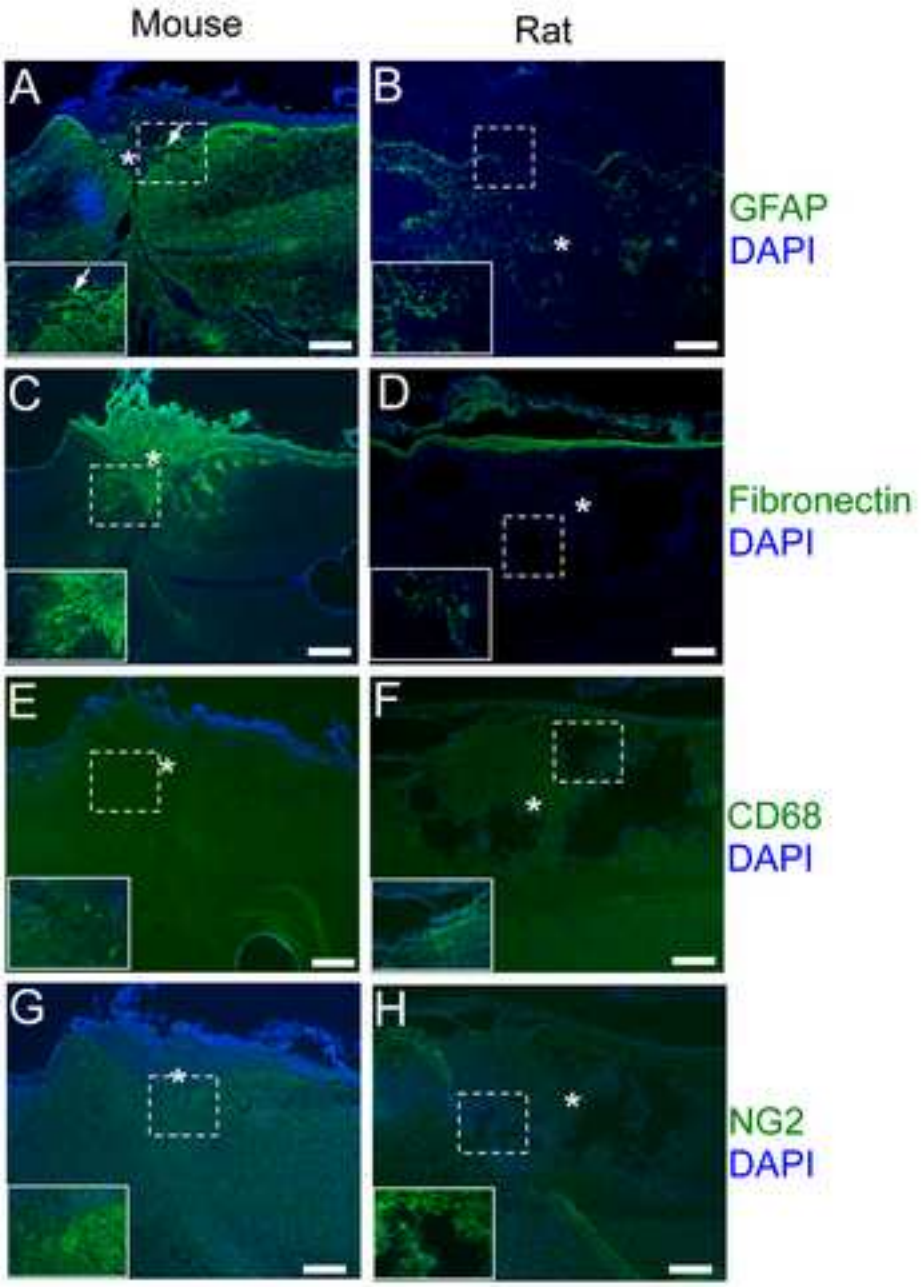

Figure 2

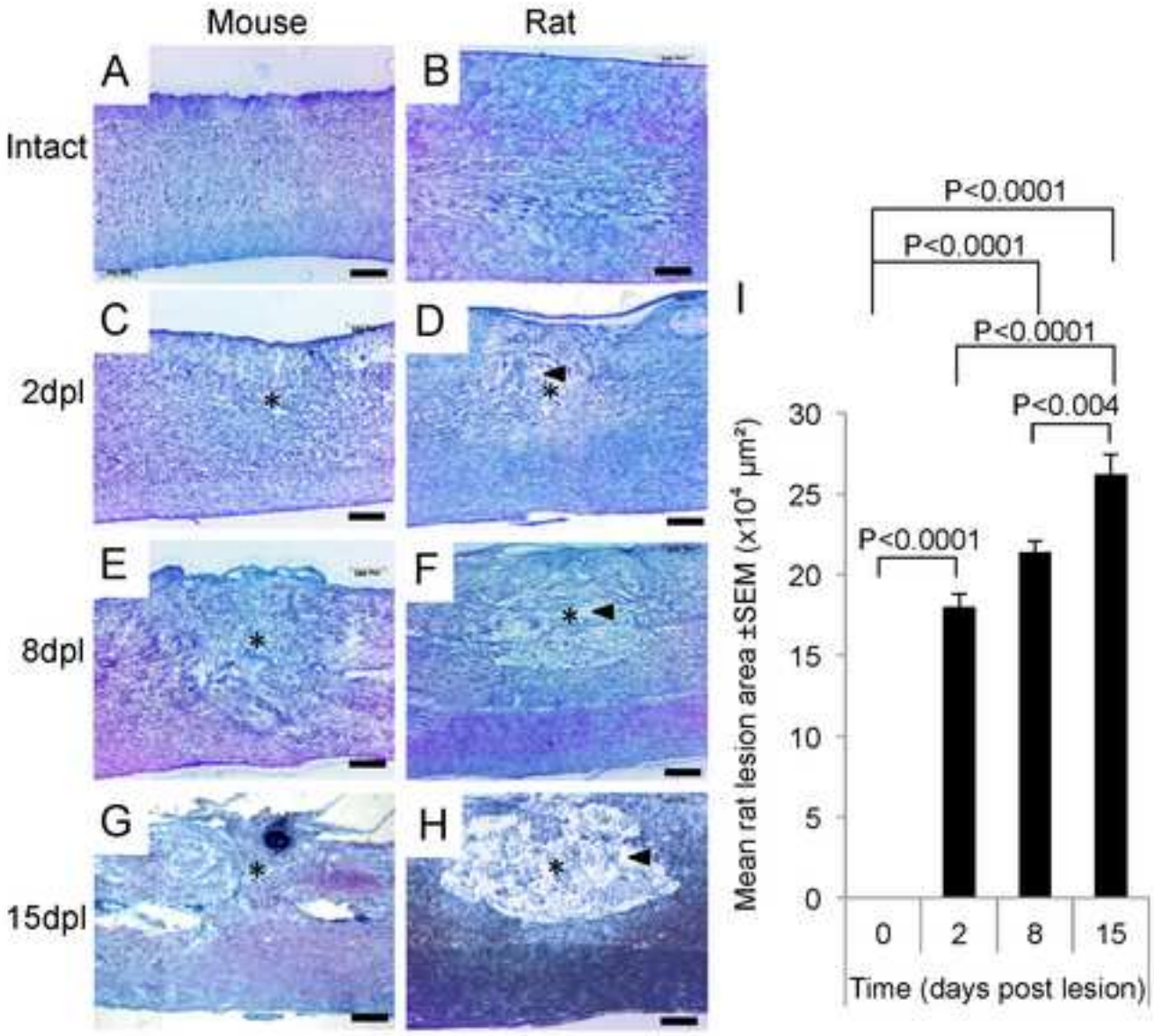
Mouse
Rat
A
B
Intact
C
D
2dpl
E
F
8dpl
G
H
15dpl
I
P<0.0001
P<0.0001
P<0.0001
P<0.004
P<0.0001
Mean rat lesion area ±SEM (x10⁴ µm²)
30
25
20
15
10
5
0
0
2
8
15
Time (days post lesion)

Figure 3

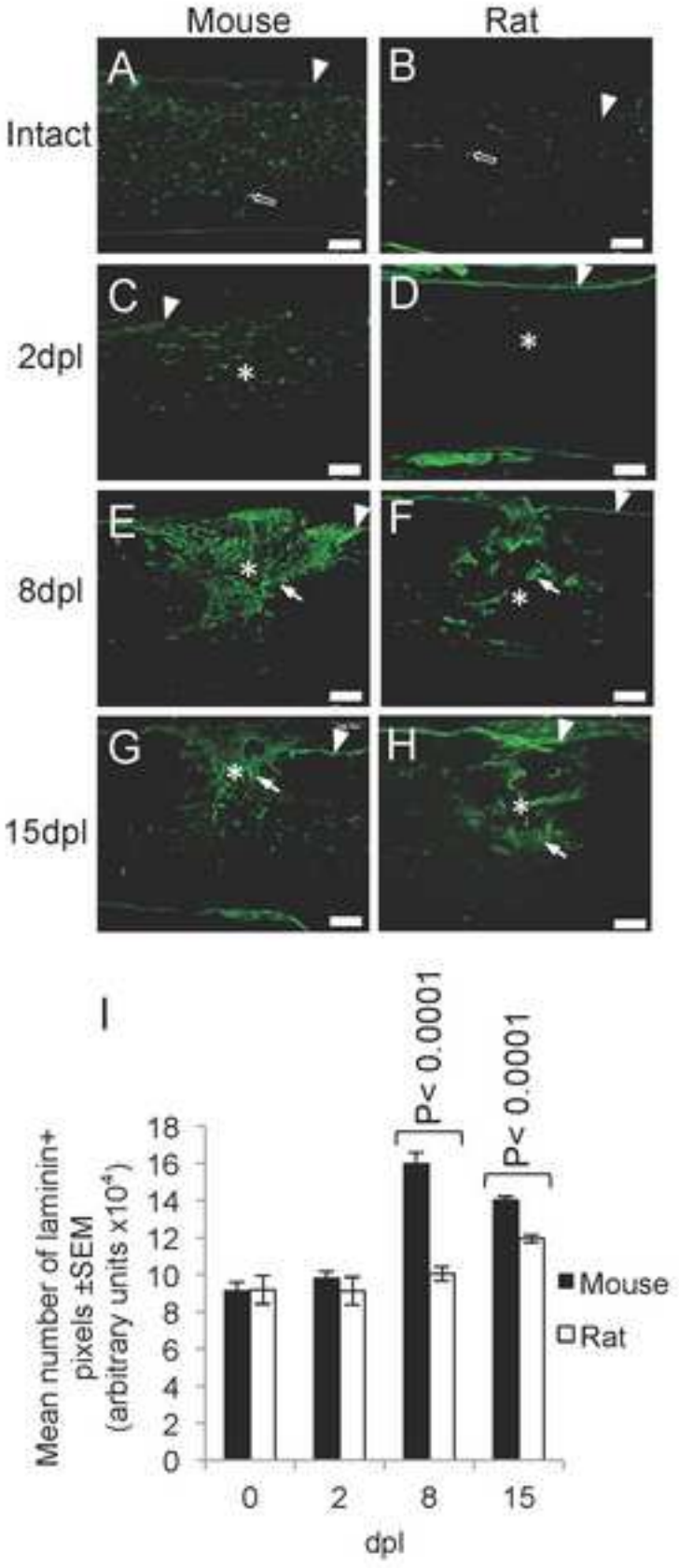
Mouse
Rat
A
B
Intact
C
D
2dpl
E
F
8dpl
G
H
15dpl
I
P< 0.0001
P< 0.0001
Mean number of laminin+ pixels ±SEM (arbitrary units x10⁴)
18
16
14
12
10
8
6
4
2
0
Mouse
Rat
0
2
8
15
dpl

Figure 4

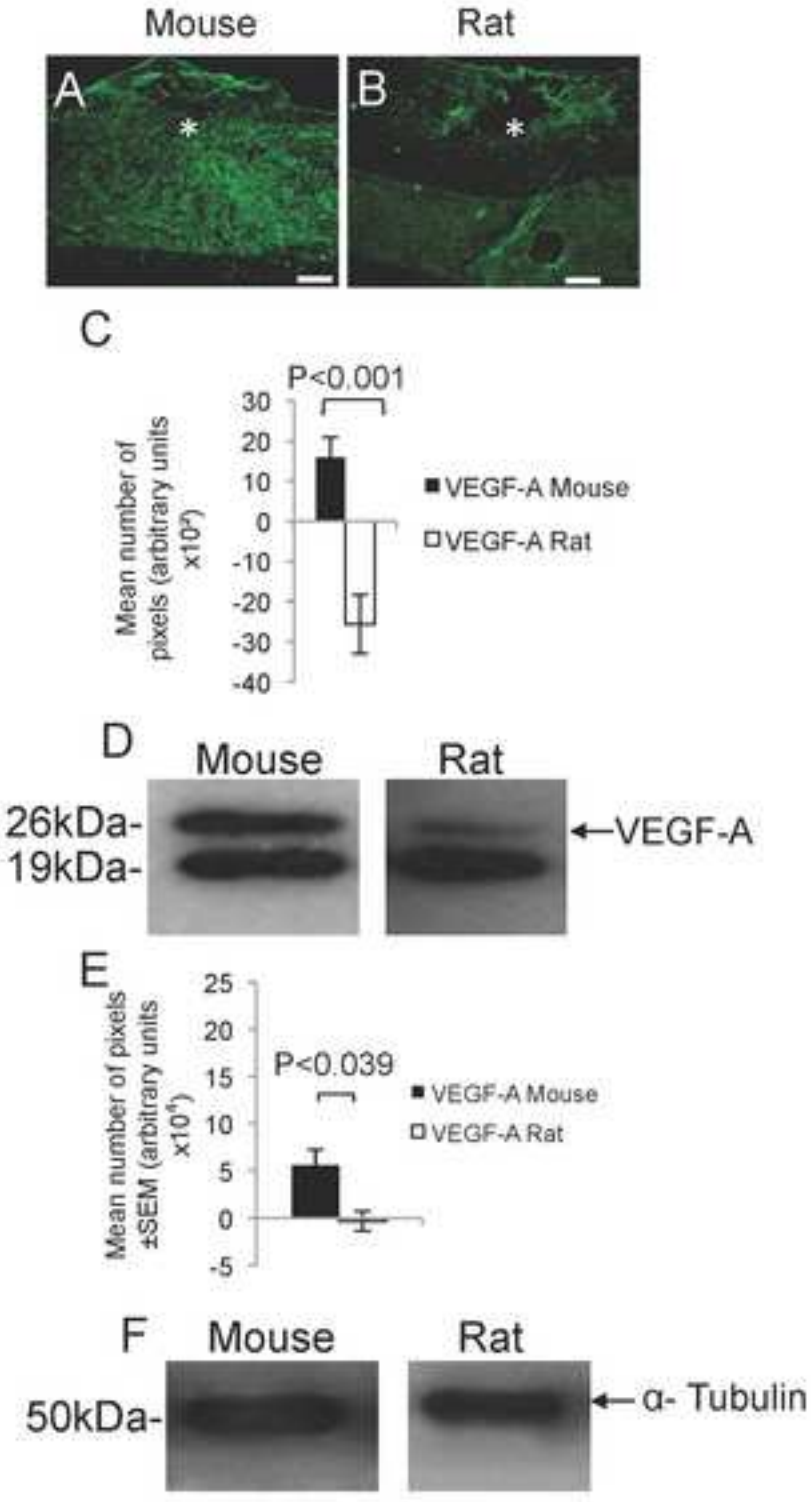
Mouse
Rat
A
B
C
P<0.001
Mean number of pixels (arbitrary units x10⁴)
30
20
10
0
-10
-20
-30
-40
VEGF-A Mouse
VEGF-A Rat
D
Mouse
Rat
26kDa-
19kDa-
VEGF-A
E
Mean number of pixels ±SEM (arbitrary units x10⁴)
25
20
15
10
5
0
-5
P<0.039
VEGF-A Mouse
VEGF-A Rat
F
Mouse
Rat
50kDa-
α- Tubulin

Figure 5

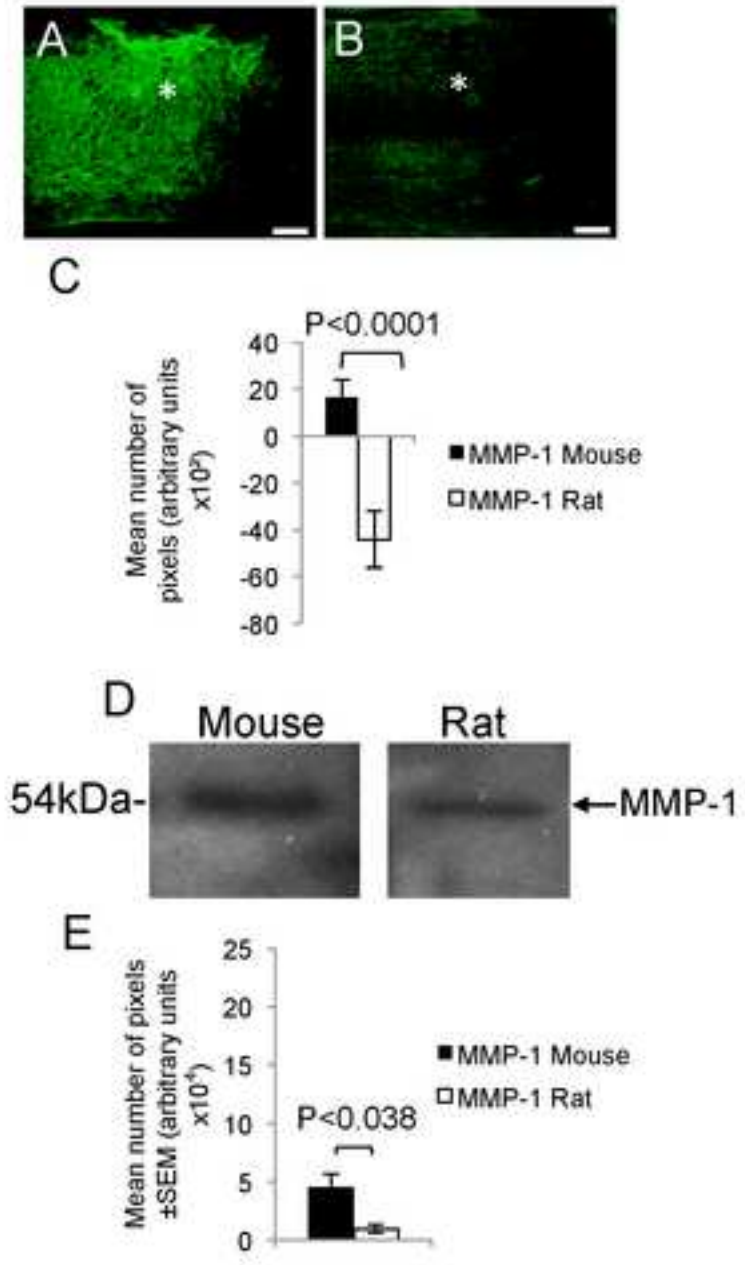

Figure 6

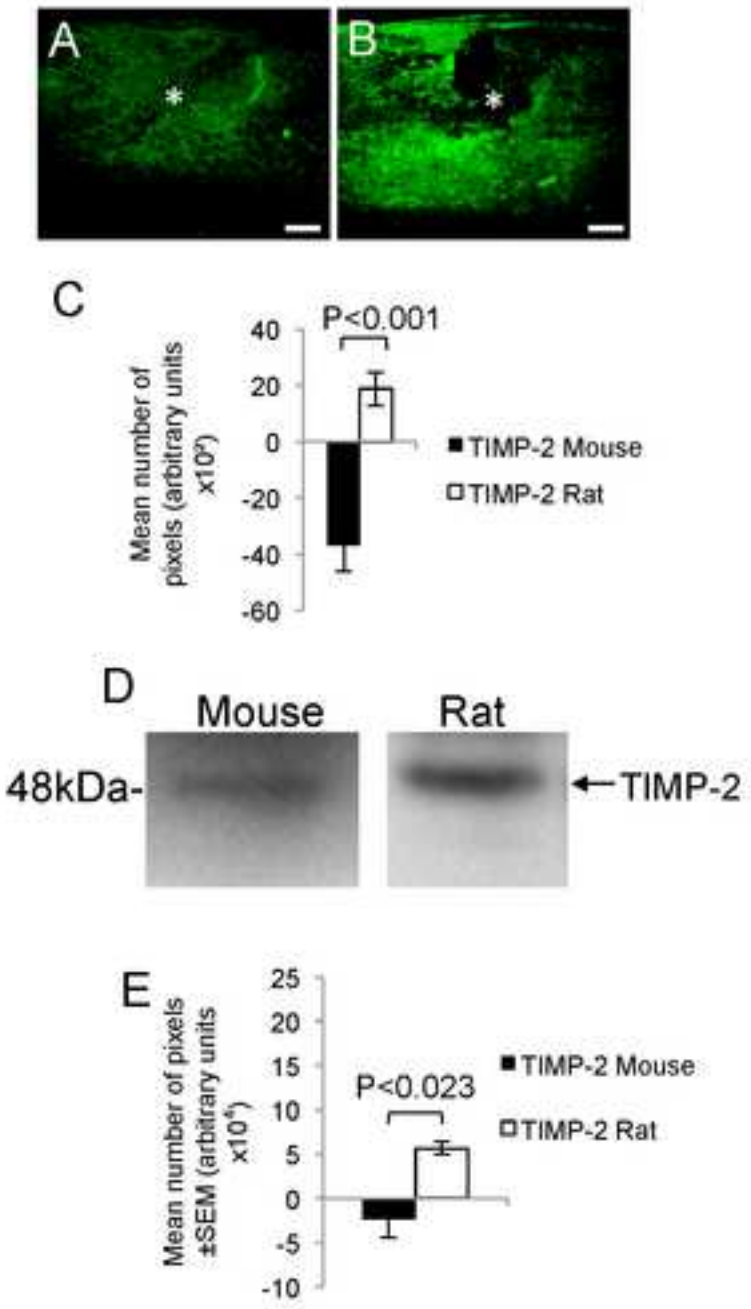

Figure 7

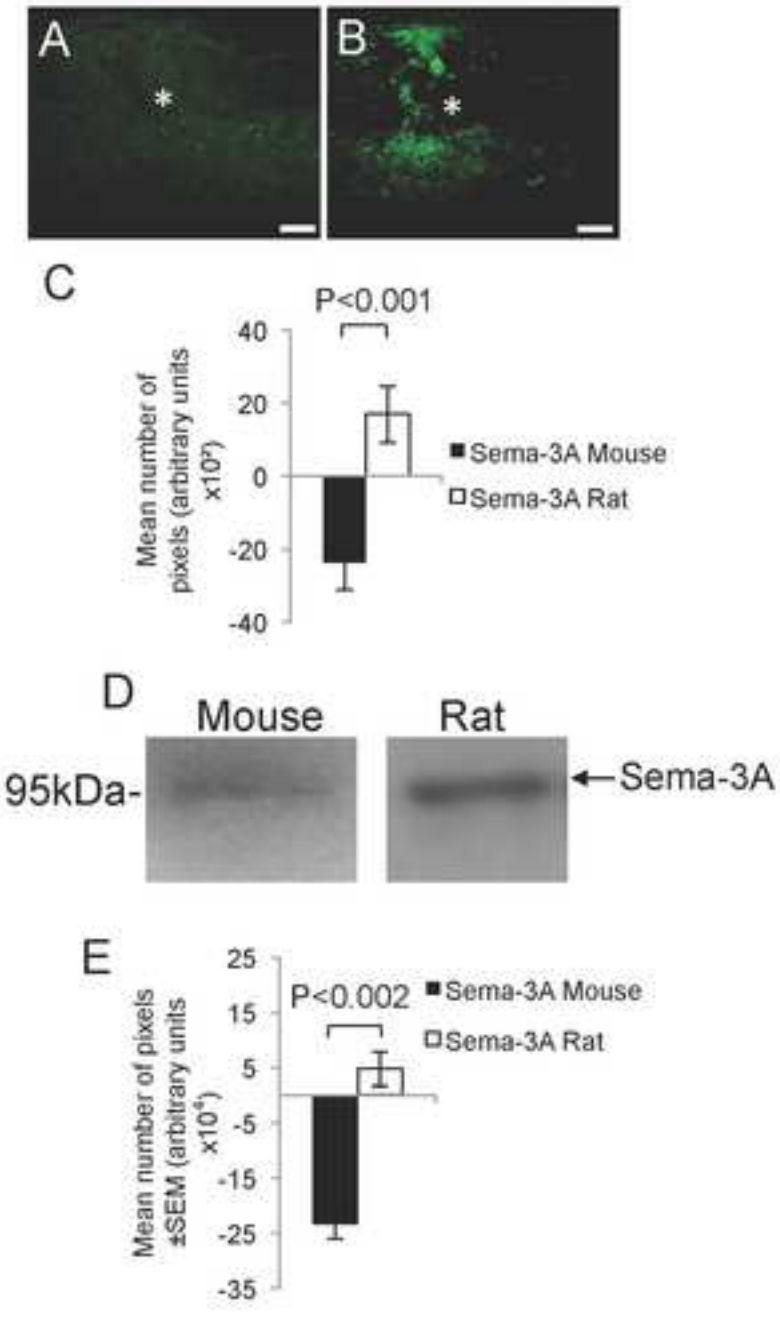

Figure 8

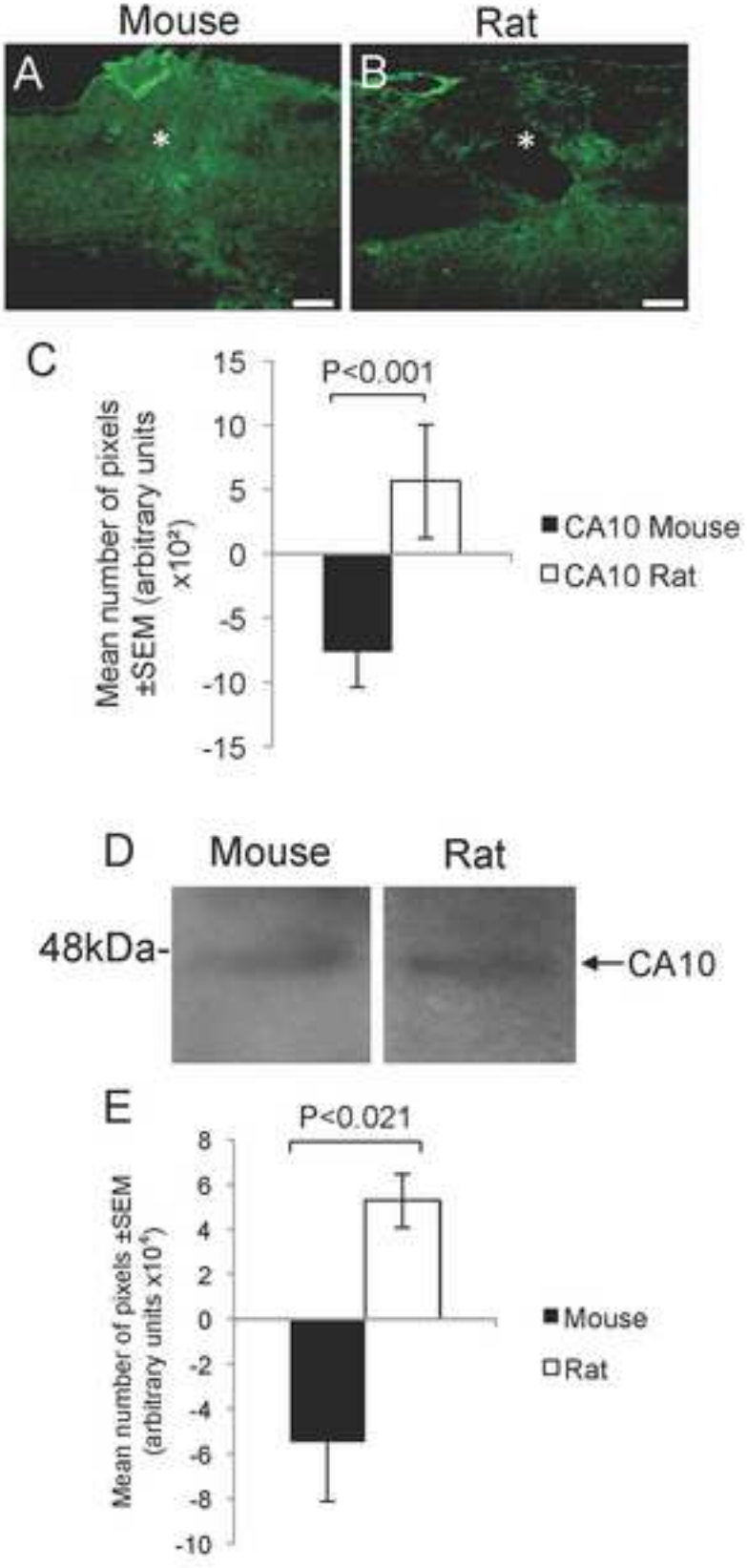
Mouse
Rat
A
B
C
P<0.001
Mean number of pixels ±SEM (arbitrary units x10²)
15
10
5
0
-5
-10
-15
CA10 Mouse
CA10 Rat
D
Mouse
Rat
48kDa-
CA10
E
P<0.021
Mean number of pixels ±SEM (arbitrary units x10⁴)
8
6
4
2
0
-2
-4
-6
-8
-10
Mouse
Rat

Figure 9

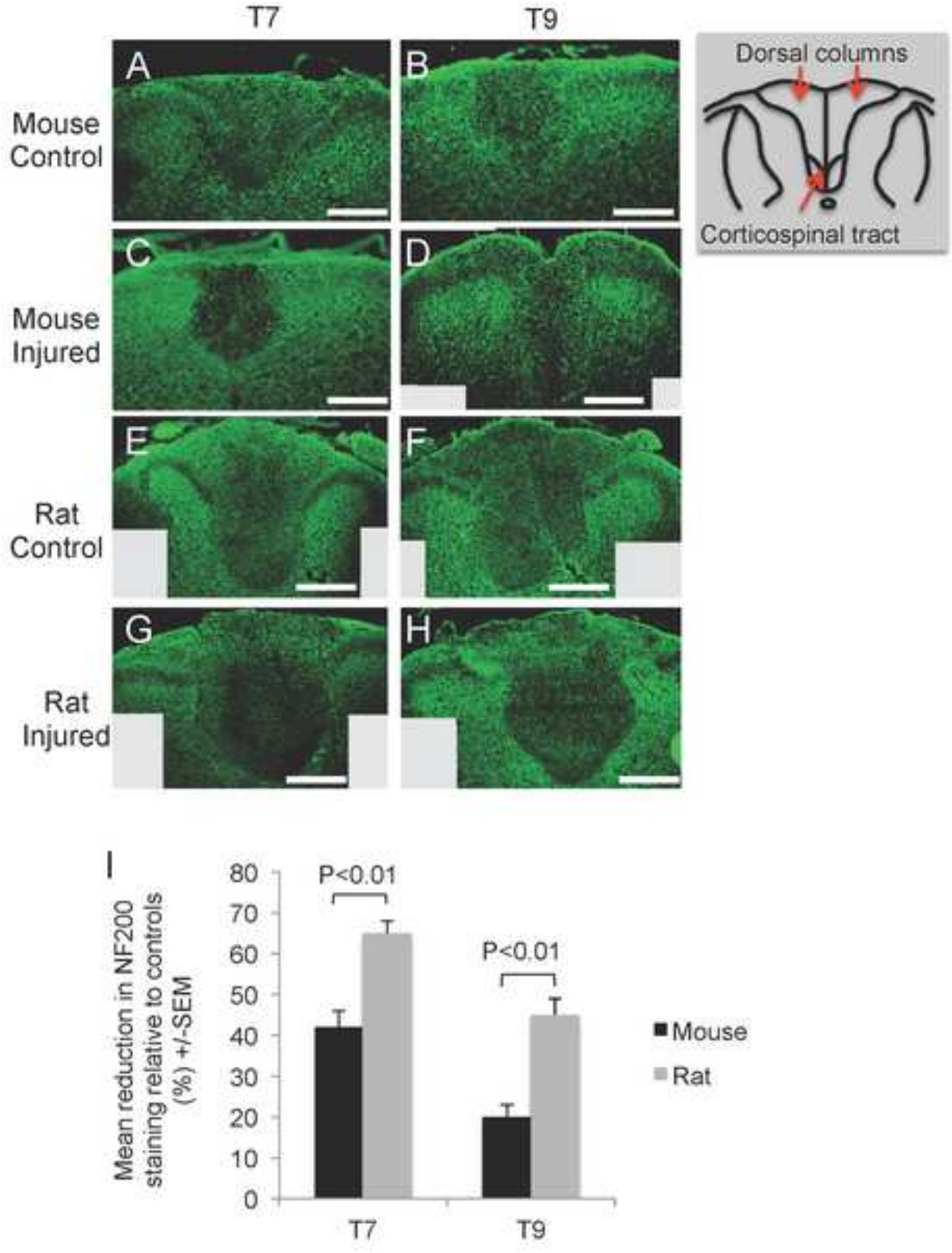
T7
T9
A
B
Mouse Control
C
D
Mouse Injured
E
F
Rat Control
G
H
Rat Injured
Dorsal columns
Corticospinal tract
I
Mean reduction in NF200 staining relative to controls (%) +/-SEM
80
70
60
50
40
30
20
10
0
P<0.01
P<0.01
T7
T9
Mouse
Rat

Figure 10

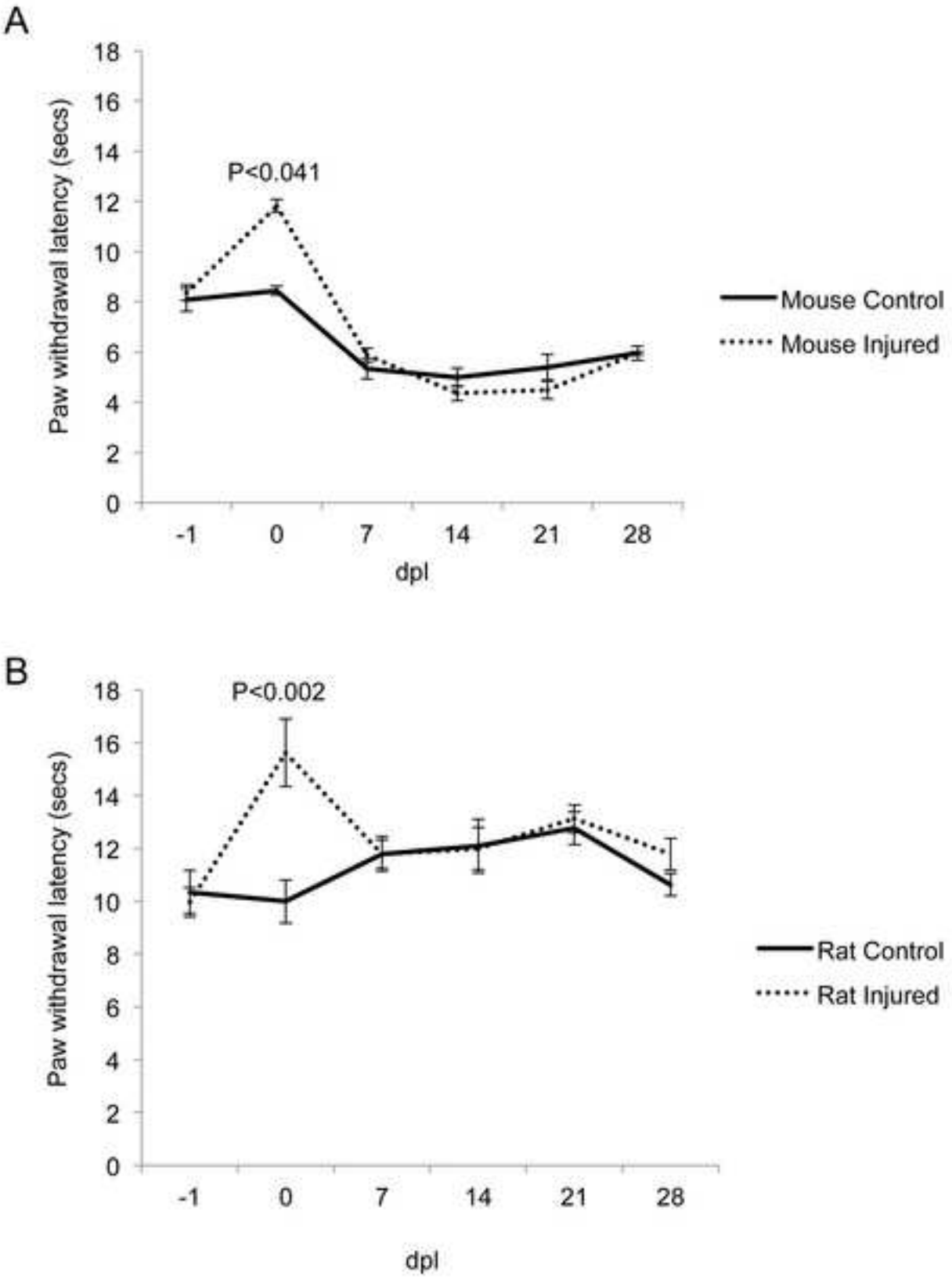
A
Paw withdrawal latency (secs)
18
16
14
12
10
8
6
4
2
0
P<0.041
-1
0
7
14
21
28
dpl
Mouse Control
Mouse Injured
B
Paw withdrawal latency (secs)
18
16
14
12
10
8
6
4
2
0
P<0.002
-1
0
7
14
21
28
dpl
Rat Control
Rat Injured

Figure 11

Table 1. List of antibodies used for this study

Angiogenic/ wound healing-related proteins	Dilution factor	Species	Supplier
Primary Antibodies			
Laminin	1:200 (IHC-F), 1:100 (WB)	Rabbit	Sigma, Poole, UK
Fibroblast growth factor (FGF2)	1:200 (IHC-F, WB)	Rabbit	Selective Genetics
Angiopoetin-1	1:200 (IHC-F), 1:100 (WB)	Rabbit	Abcam, Cambridge, UK
Semaphorin 3A	1:200 (IHC-F and WB)	Rabbit	Abcam, Cambridge, UK
Vascular endothelial growth factor A (VEGF-A)	1:400 (IHC-F), 1:1000 (WB)	Rabbit	Abcam, Cambridge, UK
Angiogenin	1:100 (IHC-F and WB)	Rabbit	Santa Cruz Biotechnology, Danvers, USA
Tissue inhibitor of metalloproteinase-2 (TIMP2)	1:200 (IHC-F and WB)	Rabbit	Neomarkers
Matrix metalloprotease-1 (MMP-1)	1:200 (IHC-F), 1:100 (WB)	Sheep	Biogenesis
Matrix metalloprotease-2 (MMP-2)	1:200 (IHC-F), 1:100 (WB)	Rabbit	Chemicon International,
Matrix metalloprotease-9 (MMP-9)	1:100 (IHC-F and WB)	Rabbit	Santa Cruz Biotechnology, Danvers, USA
Platelet endothelial cell adhesion molecule (PECAM1; CD31)	1:200 (IHC-F), 1:100 (WB)	Rabbit	Santa Cruz Biotechnology, Danvers, USA
Transforming growth factor β2 (TGFβ2)	1:200 (IHC-F and WB)	Rabbit	Santa Cruz Biotechnology, Danvers, USA
Platelet-derived growth factor (PDGF-BB)	1:200 (IHC-F and WB)	Rabbit	Chemicon,
Collagen-1	1:200 (IHC-F)	Rabbit	Abcam, Cambridge, UK
Carbonic anhydrase X	1:100 (IHC-F), 1:200 (WB)	Rabbit	Abcam, Cambridge, UK
Protein kinase C	1:250 (IHC-F)	Rabbit	Abcam, Cambridge, UK
α-tubulin	1:2000 (WB)	Rabbit	Abcam, Cambridge, UK
Secondary antibodies			
Alex 488 anti-rabbit IgG	1:400 (IHC-F)	Rabbit	
Alexa 488 anti-sheep IgG	1:400 (IHC-F)	Sheep	
Horseradish peroxidase (HRP)	1:1000 (WB)	Rabbit	

Table 2. Mean fluorescence intensities of angiogenic growth factors in sections of spinal cord at 8 dpl after DC injury.

Factor	Mean Intensity (pixels) (± SEM)		P value
	Mouse	Rat	
VEGF-A	$15 \times 10^2 \pm 5 \times 10^2$	$-25 \times 10^2 \pm 7 \times 10^2$	P<0.0001
TGFβ2	$28 \times 10^2 \pm 6 \times 10^2$	$-8 \times 10^2 \pm 4 \times 10^2$	P<0.001
PDGF-BB	$31 \times 10^2 \pm 3 \times 10^2$	$10 \times 10^2 \pm 4 \times 10^2$	P<0.002
FGF2	$6 \times 10^2 \pm 2 \times 10^2$	$-8 \times 10^2 \pm 2.5 \times 10^2$	P<0.001
Angiogenin	$19.9 \times 10^2 \pm 3 \times 10^2$	$10 \times 10^2 \pm 5.4 \times 10^2$	P<0.001
Angiopoeitin-1	$8 \times 10^2 \pm 3 \times 10^2$	$-24 \times 10^2 \pm 9 \times 10^2$	P<0.002

Table 3. Mean integrated density of angiogenic growth factors in mouse and rat SCI sites at 8 dpl, determined by western blotting.

Factor	Mean integrated density (arbitrary units) (± SEM)		P value
	Mouse	Rat	
VEGF-A	$5 \times 10^4 \pm 0.8 \times 10^4$	$-1 \times 10^4 \pm 0.6 \times 10^4$	P<0.039
TGFβ2	$2 \times 10^4 \pm 0.1 \times 10^4$	$0.5 \times 10^4 \times 0.1 \times 10^4$	P<0.001
PDGF-BB	$-9 \times 10^4 \pm 1.2 \times 10^4$	$-13 \times 10^4 \pm 0.2 \times 10^4$	P<0.045
FGF2	$17 \times 10^4 \pm 5 \times 10^4$	$1 \times 10^4 \pm 0.15 \times 10^4$	P<0.002
Angiogenin	$10 \times 10^4 \pm 0.2 \times 10^4$	$-2 \times 10^4 \pm 0.12 \times 10^4$	P<0.033
Angiopoeitin-1	$4 \times 10^4 \pm 0.8 \times 10^4$	$-3 \times 10^4 \pm 0.2 \times 10^4$	P<0.003

Table 4. Mean fluorescence intensities of MMP and TIMP in sections of spinal cord at 8 dpl after DC injury

Factor	Mean intensity (pixels) (± SEM)		P value
	Mouse	Rat	
MMP-1	$16 \times 10^2 \pm 7 \times 10^2$	$-44 \times 10^2 \pm 12 \times 10^2$	P<0.0001
MMP-2	$-19 \times 10^2 \pm 8 \times 10^2$	$-13 \times 10^2 \pm 6 \times 10^2$	P<0.425
MMP-9	$12 \times 10^2 \pm 1.7 \times 10^2$	$3 \times 10^2 \pm 2.9 \times 10^2$	P<0.007
TIMP2	$-37 \times 10^2 \pm 9 \times 10^2$	$18 \times 10^2 \pm 5.9 \times 10^2$	P<0.001

Table 5. Mean integrated density of angiogenic growth factors in mouse and rat SCI sites at 8 dpl, determined by western blotting.

Factor	Mean integrated density (arbitrary units) (± SEM)		P value
	Mouse	Rat	
MMP-1	$4.7 \times 10^4 \pm 0.05 \times 10^4$	$1 \times 10^4 \pm 0.8 \times 10^4$	P<0.038
MMP-2	$7 \times 10^4 \pm 0.5 \times 10^6$	$2.5 \times 10^4 \pm 0.05 \times 10^6$	P<0.05
MMP-9	$10 \times 10^4 \pm 0.25 \times 10^6$	$6 \times 10^6 \pm 0.07 \times 10^6$	P<0.041
TIMP2	$-2 \times 10^4 \pm 1.1 \times 10^6$	$5 \times 10^4 \pm 0.5 \times 10^4$	P<0.023

Table 6. Mean fluorescence intensities of scarring and ECM-related molecules in sections of spinal cord at 8 dpl after DC injury.

Factor	Mean Intensity (pixels) (± SEM)		P value
	Mouse	Rat	
Sema-3A	$-23 \times 10^2 \pm 7.5 \times 10^2$	$16 \times 10^2 \pm 7.6 \times 10^2$	P<0.001
Collagen-I	$20 \times 10^2 \pm 5 \times 10^2$	$-2 \times 10^2 \pm 8.5 \times 10^2$	P<0.001
PECAM-1	$23 \times 10^2 \pm 5.2 \times 10^2$	$-6.7 \times 10^2 \pm 3.5 \times 10^2$	P<0.001

Table 7. Mean integrated density of scarring and ECM-related molecules in mouse and rat SCI sites at 8 dpl, determined by western blotting.

Factor	Mean integrated density (arbitrary units) (± SEM)		P value
	Mouse	Rat	
Sema-3A	$-4 \times 10^6 \pm 1.8 \times 10^6$	$27 \times 10^6 \pm 0.87 \times 10^6$	P<0.05
Collagen-I	$24 \times 10^6 \pm 6 \times 10^6$	$-3 \times 10^6 \pm 2 \times 10^6$	P<0.001
PECAM-1	$6 \times 10^6 \pm 0.28 \times 10^6$	$0.5 \times 10^6 \pm 0.01 \times 10^6$	P<0.037

HIGHLIGHTS

- Cavitation is absent in the mouse after SCI while rats cavitate
- Absence of wound cavitation in mice correlate with increased wound healing factors
- Absence of cavities in mice correlates with enhanced axon sparing
- Robust wound healing in mice abrogates wound cavities